The SMAP Level 4 Carbon Product for Monitoring Ecosystem Land–Atmosphere CO_2 Exchange

Lucas A. Jones, *Member, IEEE*, John S. Kimball, *Senior Member, IEEE*, Rolf H. Reichle, Nima Madani, Joe Glassy, Joe V. Ardizzone, Andreas Colliander, *Senior Member, IEEE* James Cleverly, Ankur R. Desai, Derek Eamus, Eugénie S. Euskirchen, Lindsay Hutley, Craig Macfarlane, and Russell L. Scott

***Abstract*— The National Aeronautics and Space Administration's Soil Moisture Active Passive (SMAP) mission Level 4 Carbon (L4C) product provides model estimates of the Net Ecosystem CO_2 exchange (NEE) incorporating SMAP soil moisture information. The L4C product includes NEE, computed as total ecosystem respiration less gross photosynthesis, at a daily time step posted to a 9-km global grid by plant functional type. Component carbon fluxes, surface soil organic carbon stocks, underlying environmental constraints, and detailed uncertainty metrics are also included. The L4C model is driven by the SMAP Level 4 Soil Moisture data assimilation product, with additional inputs from the Goddard Earth Observing System, Version 5 weather analysis, and Moderate Resolution Imaging Spectroradiometer satellite vegetation data. The L4C data record extends from March 31, 2015 to present with ongoing production and 8–12 day latency. Comparisons against concurrent global CO_2 eddy flux tower measurements, satellite solar-induced canopy florescence, and other independent observation benchmarks show favorable L4C performance and accuracy, capturing the dynamic biosphere response to recent weather anomalies. Model experiments and L4C spatiotemporal variability were analyzed to understand the independent value of soil moisture and SMAP observations relative to other sources of input information. This analysis highlights the potential for microwave observations to inform models where soil moisture strongly controls land CO_2 flux variability; however, skill improvement relative to flux towers is not yet discernable within the relatively short validation period. These results indicate that SMAP provides a unique and promising capability for monitoring the linked global terrestrial water and carbon cycles.**

Manuscript received November 14, 2016; revised April 18, 2017; accepted June 11, 2017. This work was supported by the NASA Earth Science Program under Grant NNX14AI50G and Grant NNX15AB59G. *(Corresponding author: Lucas A. Jones.)*

L. A. Jones, J. S. Kimball, N. Madani, and J. Glassy are with the Numerical Terradynamic Simulation Group, University of Montana, Missoula, MT 59812 USA (e-mail: lucas@ntsg.umt.edu; johnk@ntsg.umt.edu).

R. H. Reichle and J. V. Ardizzone are with the NASA Global Modeling and Data Assimilation Office, Goddard Space Flight Center, Greenbelt, MD 20771 USA.

A. Colliander is with the Jet Propulsion Laboratory, California Institute of Technology, Pasadena, CA 80309 USA.

J. Cleverly and D. Eamus are with the University of Technology Sydney, Sydney, NSW 2007 Australia.

A. R. Desai is with the University of Wisconsin-Madison, Madison, WI 53706 USA.

E. S. Euskirchen is with the Institute of Arctic Biology, University of Alaska Fairbanks, Fairbanks, AK 99775 USA.

L. Hutley is with Charles Darwin University-Casaurina, NT 0909 Australia.

C. Macfarlane is with CSIRO, Floreat, WA 6014 Australia.

R. L. Scott is with the USDA Agricultural Research Service, Tucson, AZ 85719 USA.

Color versions of one or more of the figures in this paper are available online at http://ieeexplore.ieee.org.

Digital Object Identifier 10.1109/TGRS.2017.2729343

***Index Terms*— CO_2 fluxes, carbon cycle, ecosystems, environmental monitoring, microwave remote sensing, soil moisture, Soil Moisture Active Passive (SMAP) Mission, vegetation, water cycle.**

I. Introduction

SOIL moisture is a fundamental requirement of life on land. Plants and microorganisms alike require moisture for growth and turgor; accordingly, soil moisture availability plays a major role in explaining the spatial and temporal variability of the global land CO_2 sink. The land and global ocean CO_2 sinks provide a roughly 50% offset of anthropogenic atmospheric emissions with seasonal and interannual variability driven by land [1]. Attributing land sink variability is therefore key to understanding interannual changes and feedbacks to the atmospheric CO_2 growth rate. Previous studies have indicated the dominant role played by water-limited ecosystems in determining global land sink interannual variability [2]–[6]. However, quantifying global soil moisture carbon cycle interactions has been obscured by a lack of continuous, accurate soil moisture observations with global coverage at appropriate spatial and temporal resolution.

Understanding linkages between the global water and carbon cycles using global estimates of soil moisture is a major objective of the National Aeronautics and Space Administration's Soil Moisture Active Passive (SMAP) mission [7], [8]. Using soil moisture observations to improve global estimates of land CO_2 flux and evapotranspiration are a major means to this end [9]. SMAP observations are expected to have greater sensitivity to soil moisture than previously available higher frequency observations, such as those from the Advanced Scanning Microwave Radiometer and similar instruments [7]. Beginning on March 31, 2015, the SMAP satellite began providing L-band microwave brightness temperature (TB) (1.41 GHz) observations with global land surface coverage every three days. SMAP TB observations, which typically represent conditions in the top 5 cm of the soil, are assimilated into the NASA Goddard Earth Observing System, Version 5 (GEOS-5) Catchment land surface model to produce daily surface and root-zone soil moisture (SMRZ) and temperature estimates as part of the SMAP Level 4 Soil Moisture (L4SM) data product [10]–[14]. Using L4SM and other input data from GEOS-5 and the Moderate Resolution Imaging Spectroradiometer (MODIS), the SMAP Level 4 Carbon (L4C) data product provides daily global estimates of terrestrial carbon (CO_2) fluxes and underlying climatic controls [15], [16].

Soil moisture availability controls key biological processes including plant photosynthetic activity and growth, soil litter decomposition, and heterotrophic respiration (RH). Photosynthesis and gross primary production (GPP) are the primary pathways of ecosystem CO_2 uptake, whereas ecosystem respiration (RE), the sum of plant autotrophic respiration (RA) and soil RH, releases CO_2. Photosynthesis supplies the raw carbohydrate building blocks for biomass production, which eventually falls as litter and is converted into soil organic carbon (SOC). SOC is metabolized by soil microorganisms at a rate inversely proportional to the SOC carbon-to-nitrogen (C:N) ratio, or more directly the ratio of lignin to nitrogen (lignin:N), and modulated by soil moisture and temperature conditions as primary environmental control factors [17]–[19]. Whereas GPP is sensitive to plant-available soil moisture within the rooting depth profile, soil litter decomposition and RH are primarily influenced by soil moisture and temperature within the surface (0–5 cm) soil layer, where labile litter substrate (low C:N) and abundant oxygen are available [20], [18]. The physiological details of these processes are closely tied to the dominant vegetation land cover or plant functional type (PFT).

Previous satellite data-driven ecosystem modeling approaches have relied on various proxies to represent moisture constraints to ecosystem productivity and respiration, including vapor pressure deficit (VPD) to represent atmospheric moisture stress or precipitation-driven bucket models to represent plant-available soil moisture [21], [22]. The MODIS MOD17 operational GPP product uses VPD as the sole moisture constraint to vegetation productivity without accounting for its interaction with SMRZ [23]. The NASA Carnegie Ames Stanford Approach (CASA) model estimates net ecosystem CO_2 exchange (NEE) and SOC dynamics at a monthly time step and relatively coarse (0.5°) spatial resolution using a precipitation-driven bucket model to define soil moisture dynamics and environmental controls [17], [24]. The L4C product extends these previous satellite-based ecosystem models by incorporating SMAP L4SM surface and SMRZ and soil temperature information as primary environmental controls for estimating daily carbon fluxes and SOC dynamics. L4C model processing is conducted globally at 1-km resolution consistent with MODIS land cover and vegetation inputs [25]; model outputs are posted to a coarser 9-km global grid, while preserving subgrid (1-km resolution) PFT spatial heterogeneity within each grid cell.

Although soil moisture retrievals from microwave remote sensing have been available for more than a decade, relatively coarse resolution ($\geq$25 km), intermittent data coverage, large uncertainty, and variable data quality generally precluded their use within ecosystem models. Additionally, microwave measurements reflect conditions in only the surface (0–5 cm depth) soil layer. The L4SM product addresses these limitations by providing timely (latency $<$3 days), global, and temporally continuous estimates of surface-to-root zone (0–100 cm depth) soil moisture and temperature over a 9-km resolution grid, propagating surface soil information from SMAP over the entire soil profile using the GEOS-5 Catchment model [11], [14]. The L4C product integrates L4SM information within a calibrated, data-driven carbon flux model using GEOS-5 daily surface meteorology, MODIS MOD12Q1 land cover, and MOD16A2 eight-day composite observations of fraction of photosynthetically active radiation (FPAR) (the canopy-intercepted FPAR) as primary inputs. Resulting L4C product variables include NEE, GPP, RH, and surface SOC content. Additional L4C diagnostic variables include primary environmental control factors underpinning the daily carbon flux estimates and detailed quality assurance metrics describing estimated model NEE performance for every grid cell—with random error quantified as unbiased root-mean-square error (ubRMSE). Thus, the L4C product provides a new tool connecting ecosystem–atmosphere CO_2 exchange to underlying vegetation, soil moisture, and climate variability.

The overarching goals of this work are as follows:

1) To link SMAP soil moisture data to inform ecosystem CO_2 exchange and underlying environmental controls on vegetation growth, soil litter decomposition, and respiration processes using flux tower observations;
2) To determine NEE and component carbon flux sensitivity to global soil moisture variability;
3) To determine whether SMAP observations provide added value over other sources of information for estimating NEE and component carbon fluxes, including GPP and RH.

These objectives are addressed by investigating output from the L4C model after calibration to historic (pre-launch) tower flux measurements, by performing model sensitivity analyses and by evaluating the accuracy of the operational L4C data product against contemporaneous tower carbon flux measurements and other independent, global observational benchmarks.

II. Data and Methods

A. L4C Data Product

The L4C product fields are summarized in Table I. Each L4C hierarchical data format Version-5 (HDF5) daily granule contains estimates of global land–atmosphere CO_2 flux ($g{\cdot}C{\cdot}m^{-2}{\cdot}d^{-1}$), including NEE, GPP, and RH. Other L4C product fields include SOC, diagnostic environmental constraint (EC) multipliers, quality control (QC) flags, and NEE ubRMSE estimates for quality assessment (QA ubRMSE) [15], [16]. The L4C model uses a 1-km resolution EASE Grid v2 (EGv2) projection format as its native computational resolution, L4C results are posted to a coarser 9-km grid while representing major PFT categories within each grid cell averaged from the nested 1-km processing [26]. The L4C processing runs operationally within the SMAP Level 4 Science Data System of the NASA Global Modeling and Assimilation Office. The L4C system provides consistent global daily outputs with 8–12 day latency suitable for global monitoring and associated applications. Whereas L4SM latency is $<$3 days, L4C latency is further constrained by and varies with the availability of MOD16A2 FPAR eight-day composites. If MOD16A2 tiles are not received within 12 days, L4C treats the unavailable tiles as missing data and fills the missing area with an ancillary FPAR climatology. For this study, we use data from the Version 2.0, "Validated Release" L4C data product (Science

TABLE I
L4C PRODUCT DATA SETS

Group	Dataset	Units
NEE	nee_{mean, stdev}	g C m^{-2} d^{-1}
NEE	nee_pft{1..8}_mean	g C m^{-2} d^{-1}
GPP	gpp_{mean, stdev}	g C m^{-2} d^{-1}
GPP	gpp_pft{1..8}_mean	g C m^{-2} d^{-1}
RH	rh_{mean, stdev}	g C m^{-2} d^{-1}
RH	rh_pft{1..8}_mean	g C m^{-2} d^{-1}
SOC	soc_{mean, stdev}	g C m^{-2}
SOC	soc_pft{1..8}_mean	g C m^{-2}
EC	emult_mean	%
EC	tmult_mean	%
EC	wmult_mean	%
EC	frozen_area	%
QA	nee_rmse_mean	g C m^{-2} d^{-1}
QA	nee_rmse_pft{1..8}_mean	g C m^{-2} d^{-1}
QA	qa_count[a]	count
QA	qa_count_pft{1..8}[a]	count
QA	carbon_model_bitflag[b]	bit fields

Standard output datasets available in L4C daily HDF5 granules [15]. Group and Dataset names correspond to HDF5 dataset paths (See [16] for details). Brackets indicate up to eight individual datasets (e.g. {1..8}) representing each of eight global MODIS PFT vegetation classes which include: Evergreen Needleleaf Forest (1, ENF); Evergreen Broadleaf Forest (2, EBF); Deciduous Needleleaf Forest (3, DNF); Deciduous Broadleaf Forest (4, DBF); Shrubland (5, SHR); Grassland (6, GRS); Cereal Crops (6, CCR); Broadleaf Crops (7, BCR). Non-vegetated PFT classes (i.e. those not listed here; See Fig. 1) are omitted from L4C calculations. Spatial format for all datasets is 9-km EGv2 (1624 × 3856 grid cells) [26] and temporal sampling is daily unless otherwise specified in footnotes. [a]Counts are temporally static as derived by ancillary MODIS (MOD12Q1) PFT inputs (See Table II). [b]Bit flag contains several fields, some which provide static information, and others provide daily information (See [16] or HDF5 granule metadata [15] for details).

Version ID Vv2040; [15]). Three L4C data sets were used in this study: the operational L4C data set (publically available as cited above) and two scientific data sets (available upon request). Specifically, the three data sets are as follows:

1) The postlaunch operational data products(L4C Ops) spanning March 31, 2015 to present [15];
2) A prelaunch calibration, initialization, and climatological reference simulation (L4C Calib) representing the period from January 1, 2001 to December 31, 2012;
3) An "open-loop" simulation (L4C Open Loop) used to evaluate the impact of SMAP observations on postlaunch operations spanning March 31, 2015 to present [27].

Details about these data sets are provided in the following section.

B. L4C Input Data sets

L4C inputs required for model processing are summarized in Table II. The L4C model requires 1-km EGv2 static PFT and eight-day canopy FPAR maps. The L4C model also uses daily 9-km EGv2 inputs of surface soil moisture (SMSF; 0–5 cm depth), SMRZ (0–100 cm depth), surface soil temperature (TSOIL; 0–10 cm depth, except 5–15 cm for evergreen broadleaf vegetation), mean daily incoming PAR, minimum daily air temperature at 2-m height (TMIN), and mean daily VPD. The L4C Ops, L4C Calib, and L4C Open-Loop data sets derive their 9-km inputs from several native sources, including L4SM; an L4SM-emulation data set termed Nature Run Version 4 (NRv4), which is not informed by SMAP observations [10], [28]; the GEOS-5 forward processing (GEOS-5 FP) system; and the Modern Era Retrospective Reanalysis (MERRA). The L4SM, NRv4, MERRA, and GEOS-5 FP products all use similar versions of the Catchment model [29].

The native source formats of the L4C inputs are given in Table III. The L4C Ops simulation uses TSOIL and SMSF inputs from L4SM, and PAR, TMIN, and VPD from GEOS-5 FP. The L4C Calib simulations use TSOIL and SMRZ inputs from NRv4, and PAR, TMIN, and VPD from MERRA because L4SM and GEOS-5 FP data are not available for the SMAP prelaunch period. The L4C Open-Loop simulations use TSOIL and SMRZ inputs from NRv4, and PAR, TMIN, and VPD from GEOS-5 FP to isolate the impact of SMAP observations on L4C Ops. MODIS provides static PFT and eight-day FPAR inputs for each L4C simulation.

The L4SM data assimilation system provides a 3-h TSOIL and SMRZ estimates in EGv2 9-km format [11]. The 3-h L4SM data are aggregated to daily averages as an L4C preprocessing step. SMRZ in percent saturation units is rescaled to $SMRZ_{rsc}$, separately for each grid cell, using the following normalized log transforms:

$$\mathrm{SMRZ_{norm}} = 100^{*}\left(\frac{\mathrm{SMRZ}-\mathrm{SMRZ_{wp}}}{\max(\mathrm{SMRZ})-\mathrm{SMRZ_{wp}}}\right)+1 \quad (1)$$

$$\mathrm{SMRZ_{rsc}} = 95^{*}\frac{\ln(\mathrm{SMRZ_{norm}})}{\ln(101)}+5 \quad (2)$$

where max(SMRZ) is the maximum recorded soil moisture for a given grid cell and $SMRZ_{wp}$ is the plant wilting point moisture level determined by ancillary soil texture data provided by L4SM. The above rescaling improved the model calibration fit by increasing the SMRZ dynamic range, especially in arid regions where sparse rainfall may not fully saturate soil, but soil water is still accessible to arid-adapted plants.

The SMAP L4 processing system uses an Ensemble Kalman Filter (EnKF) to assimilate SMAP Level 1C orbital swath TB observations (∼36 km resolution) into the Catchment model, coupled with an L-band emission model and driven with GEOS-5 FP meteorological forcing fields [30]. Simulated soil moisture values are specific to the land model used to generate them and are typically biased with respect to the (unknown) true soil moisture [31]–[33]. This model bias in soil moisture was addressed in two steps. First, the L4SM L-band emission model was calibrated to the long-term mean of L-band TB observations from the L-band Soil Moisture Ocean Salinity (SMOS) mission [34]. The TB observations were then rescaled before the assimilation to match the seasonally varying long-term climatology of the SMOS data [35], [10]. Taken together, this means that the L4SM soil moisture analysis is driven with TB anomalies from the seasonal cycle and therefore (mostly) unbiased by construction. Because SMAP and SMOS TB observations are not cross-calibrated, some minor bias is unavoidable in the current L4SM version. Eventually, this minor bias is expected to further decrease as more SMAP data become available for model recalibration. In this study, we used input data from the Version 2 "Validated Release" L4SM data product (Science Version Vv2030) including the

TABLE II
L4C MODEL INPUT DATA

Dataset Name	Units	Input Spatial Res.[a]	L4C Ops	L4C Calib	L4C Open Loop
Plant functional Type (PFT)	Class	1-km	MOD12Q1	MOD12Q1	MOD12Q1
Fraction of absorbed PAR (FPAR)	Dim.	1-km	MOD15A2	MOD15A2	MOD15A2
Surface soil moisture (SMSF[b])	% Sat.	9-km	L4SM	NRv4	NRv4
Root zone soil moisture (SMRZ[b])	% Sat.	9-km	L4SM	NRv4	NRv4
Soil temperature (TSOIL)	K	9-km	L4SM	NRv4	NRv4
Minimum air temperature (TMIN[c])	K	9-km	GEOS-5 FP	MERRA	GEOS-5 FP
Freeze-thaw state (FT[d])	logical	9-km	GEOS-5 FP	MERRA	GEOS-5 FP
Vapor pressure deficit (VPD[e])	Pa	9-km	GEOS-5 FP	MERRA	GEOS-5 FP
Photo-synthetically active radiation (PAR[f])	W m^{-2} d^{-1}	9-km	GEOS-5 FP	MERRA	GEOS-5 FP

Daily input datasets used for the three L4C model runs (L4C Ops, L4C Calib, and L4C Open Loop). Dataset names and units are described in L4C product documentation ([16]; See text for abbreviations). Derived inputs computed from native sources (listed in Table II) as follows: [a]Spatial resolution after resampling and reformatting for L4C model grid, see Table III for native spatial resolution of each input dataset. [b]SMSF and SMRZ in % Sat. units derived by dividing by ancillary porosity data provided by L4SM or NRv4. [c]TMIN derived from daily minimum of 1-hourly T2M. [d]FT for L4C Ops was computed using daily mean of 1-hourly TSURF for this study. [e]VPD derived as the daily mean from 1-hourly PS, QV2M, and T2M. [f]PAR is derived from SWGDN assuming conversion factor of 0.45.

TABLE III
L4C INPUT DATA SOURCE NATIVE FORMAT SUMMARY

Source	Variables	Spatial Resolution	Temporal Resolution
MOD12Q1[a]	PFT	500-m	Static
MOD15A2[a]	FPAR	1-km	8-day
NRv4[b]	SMSF, SMRZ, TSOIL	9-km	3-hourly
MERRA[c]	SWGDN, QV2M, PS, T2M, TSURF,	1/2°×2/3°	1-hourly
GEOS-5 FP[c]	SWGDN, QV2M, PS, T2M, TSURF	1/4°×5/16°	1-hourly

Native sources for input data used in L4C Ops, L4C Calib, and L4C Open Loop. Dataset names are specified from original data sources (See text for abbreviations). [a]MOD12Q1 and MOD15A2 are available in sinusoidal projection tiles. [b]NRv4 spatial format is in EGv2. [c]MERRA and GEOS-5 FP spatial format is in geographic projection.

geophysical ("gph"; [11]), analysis update ("aup"; [12]), and land model constant ("lmc"; [13]) series.

The NRv4 data set was created to support the scientific development and the evaluation of SMAP Level 4 products and provides a temporally consistent data set for prelaunch model calibration and initialization and for postlaunch evaluation of the impact of SMAP observations [10], [28]. The NRv4 record was derived from 2000 to present using an identical land model to L4SM (i.e., Catchment model), but is not informed by SMAP TB observations. That is, NRv4 does not include data assimilation adjustments to the model soil moisture and temperature fields—hence, the "open-loop" designation of the corresponding L4C simulation.

The GEOS-5 FP [36] provides 3-h surface meteorological fields in $1/4° \times 5/16°$ geographic grid format, including net incoming short wave radiation (SWGDN), air temperature at 2-m height (T2M), surface skin temperature (TSURF), surface air pressure (PS), and water vapor mixing ratio at 2-m height (QV2M). The L4C preprocessor aggregates the GEOS-5 FP meteorology to a daily time step consistent with model processing. Daily PAR was estimated as a proportion (45%) of SWRAD and used with MODIS eight-day FPAR inputs to estimate canopy-absorbed PAR (APAR) on a daily basis. TMIN was computed as the daily minimum of 1-h temperature. Daily landscape freeze-thaw (FT) status was computed from TSURF using a simple pure water freezing-point threshold (273.15 K). L4C originally used SMAP radar-based FT observations, but this was abandoned due to the failure of the SMAP radar emitter on July 7, 2015. Alternative FT retrievals derived from the SMAP TB observations may be used in the future L4C versions. Daily average VPD was computed using the remaining GEOS-5 FP fields. Similar to GEOS-5 FP, MERRA input fields are available in a coarser $(1/2° \times 2/3°)$ geographic grid for the 1980–2015 record [29]. All MERRA and GEOS-5 FP fields are converted to the same 9-km EGv2 projection prior to L4C processing using nearest-neighbor resampling.

MODIS provides the fine-resolution (1 km) data used within L4C, including global land cover (MOD12Q1) and eight-day Collection 5 FPAR (MOD15A2) information available on 500-m and 1-km sinusoidal grids, respectively. The MOD12Q1 PFT (Type 5) classification [37] is resampled to 1-km EGv2 format and used in L4C model processing; the temporally static MOD12Q1 land cover classification currently used for L4C operational processing distinguishes up to eight different global PFT classes. The PFT classes were used to stratify the L4C model parameters and environmental response characteristics for different biomes. The L4C simulation was also summarized by the 1-km PFT classifications, allowing differential environmental responses within each 9-km grid cell. The MOD15A2 (Collection 5) product [38] is resampled to the 1-km EGv2 and used to define dynamic (eight days) canopy FPAR variability for L4C processing. Missing or low-quality (QC) FPAR data for a given 1-km pixel were filled prior to L4C processing using an ancillary average eight-day best QC climatology established from the MODIS historical (2001–2012) record. L4C simulations were performed only for vegetated pixels (PFT classes 1–8) with an available FPAR climatology. If MODIS 1-km FPAR observations were not available for a given eight-day period, then the ancillary 1-km FPAR climatology was substituted. Climatological FPAR substitution rates are flagged within the QA bit fields of each L4C granule if substitution rates exceed $>50\%$ for a given 9-km grid cell.

C. L4C Model Logic

NEE is defined as total RE less GPP, i.e., $\mathrm{NEE} = \mathrm{RE} - \mathrm{GPP}$, where a negative sign convention

denotes net ecosystem uptake of atmospheric CO_2. RE is computed as the sum of RA and RH. The L4C product employs a light-use-efficiency (LUE) model within a Jarvis-Stewart constraint framework for estimating GPP [39]–[42]. Many previous LUE formulations are available [43]; however, the L4C model combines LUE and soil decomposition models to determine a more comprehensive daily carbon budget, using daily rescaled SMRZ inputs to constrain GPP, daily SMSF inputs to constrain RH, and employs model calibration using historical daily CO_2 flux observations from the global tower (FLUXNET) observation network. The L4C LUE model is as follows:

$$\mathrm{GPP} = \mathrm{APAR}^{*}\varepsilon_{\max}{}^{*}E_{\mathrm{mult}} \tag{3}$$

$$E_{\mathrm{mult}} = f_{\mathrm{EC}}(\mathrm{VPD})\, f_{\mathrm{EC}}(\mathrm{TMIN})\, f_{\mathrm{EC}}(\mathrm{SMRZ})\, f_{\mathrm{EC}}(\mathrm{FT}) \tag{4}$$

where canopy-APAR is defined as the product of PAR and FPAR; $\varepsilon_{\max}$ is a maximum LUE parameter defined for individual PFT classes under optimal (nonlimiting) environmental conditions; and E_{mult} is the relative reduction in estimated photosynthetic LUE from its potential ($\varepsilon_{\max}$) due to suboptimal environmental conditions. Limiting conditions include excessive VPD, low TMIN, frozen conditions, or low SMRZ. Emult is defined as the product of equally weighted dimensionless (0–1) scalar multipliers representing PFT-specific responses to each environmental variable. The $f_{\mathrm{EC}}(x)$ terms in (4) are described using linear ramp functions ranging from optimal (1) to fully constrained (0) conditions [23] for each environmental variable

$$f_{\mathrm{EC}}(x) = \begin{cases} 1 & \text{if } x \geq x_{\max}, \\ 0 & \text{if } x \leq x_{\min}, \\ (x - x_{\min})/(x_{\max} - x_{\min}) & \text{otherwise} \end{cases} \tag{5}$$

where x is VPD, TMIN, or SMRZ, with $x_{\min}$ and $x_{\max}$ as model parameters specified for each PFT class [25]. These parameters determine the effective slope of $f_{\mathrm{EC}}(x)$ between fully constrained ($f_{\mathrm{EC}}(x) = 0$), and fully unconstrained ($f_{\mathrm{EC}}(x) = 1$) conditions, and do not necessarily correspond with the absolute minimum and maximum values of x. The FT constraint $f_{\mathrm{EC}}(\mathrm{FT})$ is either zero if frozen or unity if nonfrozen. RA is then computed as the PFT prescribed fraction (f_{aut}) of estimated GPP (i.e., RA = f_{aut} GPP; [44]).

RH is estimated using a three-pool soil decomposition model with cascading SOC quality and associated decomposition rates. Carbon fixed from atmospheric CO_2 by GPP enters the SOC pools as litterfall (L_{fall}) specified as a constant daily fraction of estimated mean annual net primary productivity (NPP = GPP − RA). Daily SOC change for each of the three SOC pools is specified as [25], [42], [45]

$$\frac{dC(t)_{\mathrm{fast}}}{dt} = L_{\mathrm{fall}}\mathrm{f}_{\mathrm{fast}} - \mathrm{RH}(t)_{\mathrm{fast}} \tag{6}$$

$$\frac{dC(t)_{\mathrm{med}}}{dt} = L_{\mathrm{fall}}(1 - f_{\mathrm{fast}}) - \mathrm{RH}(t)_{\mathrm{med}} \tag{7}$$

$$\frac{dC(t)_{\mathrm{slow}}}{dt} = \mathrm{f}_{\mathrm{med}}\mathrm{RH}(t)_{\mathrm{med}} - \mathrm{RH}(t)_{\mathrm{slow}} \tag{8}$$

where subscripts denote typical SOC decay rates relating to labile (e.g., leaves and fine roots with low C:N), structural (e.g., coarse woody roots with moderate C:N and high lignin content), and recalcitrant (e.g., high C:N, tannins, phenols, SOC bound in clay, and permafrost) SOC pools, respectively. RH is computed for the ith SOC pool in (6)–(8) using SMSF and soil temperature as primary controls on SOC decomposition [42]

$$\mathrm{RH}_i(t) = f_{\mathrm{EC}}(\mathrm{TSOIL})\, f_{\mathrm{EC}}(\mathrm{SMSF}) k_i C_i(t) \tag{9}$$

where $f_{\mathrm{EC}}(\mathrm{TSOIL})$ is an Arrhenius exponential function of TSOIL from [46]; $f_{\mathrm{EC}}(\mathrm{SMSF})$ is a ramp function of SMSF (0–5 cm); and k_i is the optimal decay rate for the ith SOC pool. Total RH is derived as the sum of RH_i, including the adjustment $\mathrm{RH}_2 = (1 - f_{\mathrm{med}})\mathrm{RH}_{\mathrm{med}}$ to account for material transferred into the slow pool during humification [17].

Random error uncertainty estimates for NEE–indicated by the ubRMSE metric–are produced using analytical error propagation. We define the ubRMSE of two random variables as the variance of the residuals of their least-squares regression. We then compute the Jacobian ($\mathbf{J}$) by taking derivatives of NEE of the above model with respect to each input data set. We then assign a diagonal input error covariance matrix ($\mathbf{E}_{\mathrm{input}}$) as part of the L4C calibration process (Section II-C). The estimated NEE error is then computed as

$$E_{\mathrm{NEE}}(t) = \mathbf{J}(t)\mathbf{E}_{\mathrm{input}}\mathbf{J}^{\mathbf{T}}(t) \tag{10}$$

for each 1-km pixel and daily time step. The now scalar quantity E_{NEE} term is spatially averaged using the sum of squares within each 9-km grid cell and the NEE ubRMSE QA metric is computed as the square root of this average.

D. Model Calibration and Initialization

The L4C model was calibrated during the mission prelaunch phase using a global network of *in situ* tower eddy covariance CO_2 flux measurement records (2000–2008) from the FLUXNET La Thuile Collection [47], [48]. This data set consists of 238 flux tower locations, representing the major global biomes and PFT classes, although spatial coverage heavily favors temperate forest and cropland ecosystems in the United States and Europe [48]. We used only tower sites having at least two years of observations, leaving 228 remaining sites (Fig. 1). We used daily NEE, GPP, and RE computed from half-hourly NEE as reported by the La Thuile site investigators. Daily GPP and RE estimates were partitioned from half-hourly NEE measurements based on the short-term temperature response of respiration to nighttime NEE [49], [50]. Since gap filling of flux data requires preassigned meteorological responses, we used only daily data values reported as nongap filled.

Model calibration proceeded in three steps using daily eddy covariance CO_2 flux observations from the 228 tower calibration sites stratified by their dominant PFT coverage:

1) The L4C GPP model outputs were fitted to the selected tower GPP observations.
2) The RE model outputs were then fitted to the tower RE observations using the new estimates from the calibrated GPP model.
3) The NEE ubRMSE estimates were then fitted to NEE RMSE computed using the newly calibrated model NEE versus the tower NEE observations.

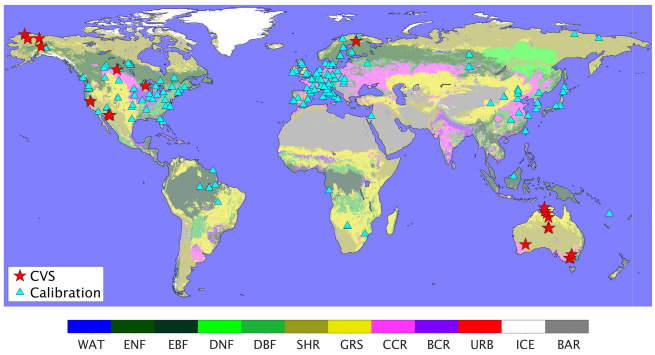

Fig. 1. CVS and calibration tower sites used for evaluating operational L4C results and for prelaunch the L4C model calibration, respectively. Base map shows global PFTs from the MODIS Collection 5 global land cover classification (MOD12Q1 Type 5). PFT abbreviations (as in Tables I and III): WAT = water; ENF = evergreen needleleaf forest; EBF = evergreen broadleaf forest; DNF = deciduous needleleaf forest; DBF = deciduous broadleaf forest; SHR = shrubland; GRS = grassland; CCR = cereal crops; BCR = broadleaf crops; URB = urban; ICE = permanent snow/ice; and BAR = barren.

The three steps were repeated for each of the eight vegetated PFT categories. The L4C model fitted parameters for GPP included $\varepsilon_{\max}$, $\mathrm{VPD}_{\min}$, $\mathrm{VPD}_{\max}$, $\mathrm{TMIN}_{\min}$, $\mathrm{TMIN}_{\max}$, $\mathrm{SMRZ}_{\min}$, and $\mathrm{FT}_{\mathrm{mult}}$; the model RE fitted parameters included F_{aut}, and $\mathrm{SMSF}_{\min}$. The model parameters were confined to predefined realistic bounds and were fixed at default values if extremes were not well represented by the tower calibration sites (e.g., VPD for tropical EBF rarely exceeds 3 kPa). Tower flux data from multiple locations were pooled according to the dominant (highest coverage) PFT of the 9-km model grid cell overlying each tower location, and model parameters were calibrated separately for each PFT class. The towers used for the model calibration were also screened to ensure consistency between the dominant PFT represented within the tower footprint and the overlying 9-km model grid cell. All optimizations were fitted using nonlinear least-squares regression.

The L4C model SOC values were initialized to steady-state conditions during the SMAP prelaunch phase using the daily input mean seasonal cycle across years (i.e., climatology). The resulting L4C NEE source/sink strength thus depends on the effective differences of current conditions versus those from the recent (2001–2012) period used to define the SOC pool available for decomposition and RH. Because most ecosystems are not in steady state [48], [51], L4C tends to underestimate the effective carbon sink strength indicated from tower observations. Therefore, L4C RE and NEE are high biased and low biased, respectively, relative to most tower observations in undisturbed ecosystems [51]. To mitigate these site-to-site biases when calibrating RE against tower data, we determine the 95th percentile of RE from each tower site and substitute this quantity as a constant effective SOC factor ($\bar{C}$) during L4C model calibration

$$\bar{C} \cong \sum k_i C_i. \tag{11}$$

Summing (11) and substituting (9), total RH can now be expressed as

$$\mathrm{RH}(t) = f_{\mathrm{EC}}(\mathrm{TSOIL})\, f_{\mathrm{EC}}(\mathrm{SMSF})\bar{C} \tag{12}$$

which simplifies calibration by combining unidentifiable rate and effective storage parameters until a single constant factor for each site. This procedure is imperfect because C_{fast} is seasonally dynamic (i.e., has subannual turnover time), but for practical purposes, it reduces the effective model bias during calibration.

After calibration, L4C SOC levels were initialized to steady-state conditions using two steps. In the first step, we analytically solved (6)–(8) using the L4C Calib inputs. This solution provided steady-state annual mean SOC values. In the second step, these values were used to initialize a numerical solution (i.e., "spin-up"), which cycles the input MERRA, NRv4, and FPAR climatologies until the annual NEE is within ± 1 g·C·m^{-2}·y^{-1}. Since the analytical values were quite close to the numerical steady state (closer for C_{slow} than C_{fast}, because C_{fast} has a larger seasonal cycle), this procedure usually required only a few ($\leq$10) annual cycles. This is resulted in a global 1-km SOC map for each day of a climatological year, which was then used to initialize L4C Ops for the March 31, 2015 beginning of the SMAP operational record.

E. Multitier Validation Strategy

The targeted performance metric for the L4C product is to estimate NEE at the level of uncertainty commensurate with *in situ* tower measurement-based observations (ubRMSE $\leq$ 1.6 g·C·m^{-2} d^{-1} or 30 g·C·m^{-2}·y^{-1}). The L4C product accuracy was primarily assessed against independent CO_2 flux measurement-based observations from a global network of 26 core tower validation sites (CVS) having concurrent overlapping observations with the L4C operational record for the March 31, 2015 to December 31, 2015 period (Table IV; Fig. 1). The L4C operational product was also verified against other similar global observational benchmarks, including Solar-Induced canopy Fluorescence (SIF) from the ESA GOME-2 sensor on the MetOp-A and MetOp-B satellites, which was used as a proxy for GPP [52]. GOME-2 provides Level 3 global monthly 734 –758 nm (Channel 4, version 26) SIF retrievals on a 0.5° × 0.5° grid extending from 2007 to present [53]. The GOME-2 record was selected for this study over other SIF observations, including the NASA Orbiting Carbon Observatory (OCO2) [54], because of the longer record and consistent global gridding available from GOME-2. We also compared L4C effective NEE source/sink patterns against alternative NEE estimates derived from NOAA CarbonTracker atmospheric transport model inversions of global CO_2 flask measurements [24]. CarbonTracker estimates continental-scale land and ocean carbon flux magnitudes using an EnKF to assimilate atmospheric CO_2 flask measurements into TM-5 wind transport simulations using estimates of anthropogenic and fire CO_2 emissions. CarbonTracker's biospheric flux subcontinental spatial patterns are based on the GFED-CASA land model, which provides both NEE prior conditions and estimated fire CO_2 emissions, whereas continental-scale flux magnitudes are adjusted for individual ecoregions using the CarbonTracker atmospheric inversion [24], [55]. Comparing L4C NEE with CarbonTracker

TABLE IV
TOWER CVS USED FOR L4C VALIDATION ASSESSMENT

Site	Name	PFT	Location	Lat.	Lon.	PI	Affiliation
FI-Sod[a]	Sodankyla	ENF	Finland	67.36 °N	26.64 °E	M. Aurela	Finnish Meteorol. Institute
CA-Oas	SK-Old Aspen	DNF	SK, Canada	53.63 °N	106.20 °W	H. Wheater	U. Saskatchewan
US-ICt	Imnavait Creek Tussock	SHR	AK, USA	68.61 °N	149.30 °W	E. Euskirchen	U. Alaska-Fairbanks
US-ICh	Imnavait Creek Heath	SHR	AK, USA	68.61 °N	149.30 °W	E. Euskirchen	U. Alaska-Fairbanks
US-ICs	Imnavait Creek Sedge	SHR	AK, USA	68.61 °N	149.31 °W	E. Euskirchen	U. Alaska-Fairbanks
US-PFa	Park Falls WLEF Tall Tower	DBF	WI, USA	45.95 °N	90.27 °W	A. R. Desai	U. Wisconsin-Madison
US-BZs	Bonanza Creek Spruce	ENF	AK, USA	64.70 °N	148.32 °W	E. Euskirchen	U. Alaska-Fairbanks
US-BZb	Bonanza Creek Bog	ENF	AK, USA	64.70 °N	148.32 °W	E. Euskirchen	U. Alaska-Fairbanks
US-BZf	Bonanza Creek Fen	ENF	AK, USA	64.70 °N	148.31 °W	E. Euskirchen	U. Alaska-Fairbanks
US-Atq	Atqasuk	GRS	AK, USA	70.47 °N	157.40 °W	W. Oechel	San Diego State U.
US-Ivo	Ivotuk	SHR	AK, USA	68.47 °N	155.73 °W	W. Oechel	San Diego State U.
US-SRM	Santa Rita Mesquite	SHR	AZ, USA	31.82 °N	110.87 °W	R. L. Scott	USDA Agric. Research Service
US-Wkg	Walnut Gulch Kendall Grassland	GRS	AZ, USA	31.74 °N	109.94 °W	R. L. Scott	USDA Agric. Research Service
US-Whs	Walnut Gulch Lucky Hills	SHR	AZ, USA	31.74 °N	110.05 °W	R. L. Scott	USDA Agric. Research Service
US-Ton	Tonzi Ranch	SHR	CA, USA	38.43 °N	120.97 °W	D. Baldocchi	U. California-Berkeley
US-Var	Vaira Ranch	SHR	CA, USA	38.41 °N	120.95 °W	D. Baldocchi	U. California-Berkeley
AU-Whr	Whroo	SHR	Australia	36.67 °S	145.03 °E	J. Beringer	U. Western Australia
AU-Rig	Riggs Creek	CCR	Australia	36.65 °S	145.58 °E	J. Beringer	U. Western Australia
AU-Ync	Yanco	CCR	Australia	34.99 °S	146.29 °E	J. Beringer	U. Western Australia
AU-Stp	Sturt Plains	GRS	Australia	17.15 °S	133.35 °E	J. Beringer L. Hutley	U. Western Australia, Charles Darwin U.
AU-Dry	Dry River	GRS	Australia	15.26 °S	132.37 °E	J. Beringer L. Hutley	U. Western Australia, Charles Darwin U.
AU-DaS	Daly River Uncleared Savannah	GRS	Australia	14.16 °S	131.39 °E	J. Beringer L. Hutley	U. Western Australia, Charles Darwin U.
AU-How	Howard Springs	GRS	Australia	12.50 °S	131.15 °E	J. Beringer L. Hutley	U. Western Australia, Charles Darwin U.
AU-GWW[a]	Great Western Woodlands	SHR	Australia	30.19 °S	120.65 °E	C. Macfarlane	CSIRO
AU-ASM	Alice Springs	SHR	Australia	22.28 °S	133.25 °E	J. Cleverly, D. Eamus	U. Technology, Sydney
AU-TTE	Ti Tree East	SHR	Australia	22.29 °S	133.64 °E	J. Cleverly, D. Eamus	U. Technology, Sydney

CVS eddy covariance flux tower site and principle investigator (PI) list. Investigators from these 26 sites made data available which met requirements for temporal overlap with the SMAP L4C data record from March 31, 2015 to December 31, 2015. Site names and abbreviations as provided by FLUXNET. PFT for each tower location was determined by the overlying MOD12Q1 1-km pixel. Shading indicates adjacent tower site records which share the same L4C 9-km grid cell. [a]RE flux estimates not available. See Table I for PFT explanation of PFT abbreviations.

biospheric flux provides an atmospheric perspective and a means for evaluating L4C potential to inform the future inversion studies.

The L4C SOC outputs were compared with independent SOC estimates derived from global and regional soil inventory records, including the International Geosphere-Biosphere Data and Information System (IGBP-DIS) global [56] and the Northern Circumpolar Soil Carbon Database (NCSCD) SOC maps [57]. Within the soil column, the largest SOC levels are generally found within surface soil layers, declining exponentially with depth [58]. The IGBP-DIS and NCSCD SOC values represent the top 1-m soil layer and were systematically decreased by a factor of 1/3 to approximate surface ($<$10 cm) soil conditions represented by the L4C SOC outputs.

We performed two types of model sensitivity analyses to quantify the impact of soil moisture on the L4C-derived global carbon fluxes. First, we ran L4C Calib using the daily climatology inputs and removed the model soil moisture constraints to investigate their individual impact on the L4C estimated annual GPP and RH fluxes. Since RE is impacted by both GPP and RH, we focus on GPP and RH (rather than RE) to decouple their differential responses to soil moisture. Second, to assess the impact of SMAP observations on the carbon model calculations, we compared the L4C Ops record against L4C Open-Loop simulations derived using NRv4 inputs without the influence of SMAP [27]. The L4C Ops, L4C Open Loop, and L4C Calib results were then evaluated against the CVS tower daily carbon flux observations. A guiding hypothesis for the model sensitivity analysis was that the SMAP informed L4C Ops simulations should show similar or better accuracy than the L4C Open-Loop simulations derived without the benefit of SMAP observations. Likewise, L4C Ops should also outperform the L4C Calib climatological predictions. A similar approach was employed by the L4SM team to evaluate impacts of the L4SM data assimilation [14]. Combining these two types of analysis, we also compute the global interannual variance of L4C Calib and compare this quantity to global differences between L4C Ops and L4C Open Loop to investigate how SMAP information may inform L4C global interannual variability.

III. RESULTS

A. Comparison With Core Flux Sites

The L4C Ops overall mean NEE RMSE was 1.04 $g{\cdot}C{\cdot}m^{-2}{\cdot}d^{-1}$, and NEE ubRMSE was 0.79 $g{\cdot}C{\cdot}m^{-2}{\cdot}d^{-1}$ relative to the CVS tower carbon flux benchmark measurements (Table V). The SMAP L4C-targeted accuracy threshold is ubRMSE $\leq$ 1.6 $g{\cdot}C{\cdot}m^{-2}{\cdot}d^{-1}$ mean across all sites, so the overall site mean NEE ubRMSE is within this threshold. The L4C GPP results showed the highest correlation with the tower observations, followed by RE,

TABLE V
L4C VALIDATION SUMMARY STATISTICS FROM THE CVS COMPARISONS

Flux	R			RMSE			ubRMSE		
L4C Run	Ops	OL	Calib	Ops	OL	Calib	Ops	OL	Calib
NEE	0.52	0.52	0.48	1.04	1.05	1.01	0.79	0.79	0.80
GPP	0.72	0.72	0.71	1.27	1.31	1.21	0.85	0.85	0.83
RE	0.65	0.65	0.66	1.16	1.20	1.10	0.62	0.62	0.62

NEE, GPP, and RE statistics represent means taken across 26 tower sites (26 sites for NEE and GPP with 24 sites for RE) including locations shown in Fig. 1 and corresponding to individual site statistics given in Fig. 2. L4C model runs abbreviated as follows: Ops indicates L4C with L4SM inputs (L4C Ops); OL indicates L4C with NRv4 inputs (L4C Open Loop); and Calib indicates L4C with NRv4 (L4C Calib) climatology inputs. R = Pearson correlation, RMSE = root mean square error, ubRMSE = un-biased RMSE.

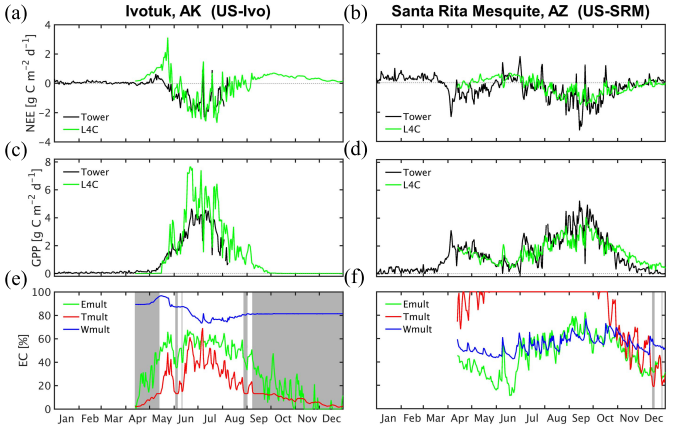

Fig. 2. Time series of L4C Ops fields and tower observations (if available) for selected tower locations: US-Ivo (Alaska arctic tundra) and US-SRM (Arizona desert shrubland). Fields include (a) and (b) NEE, (c) and (d) GPP, and (e) and (f) L4C EC, including GPP LUE constraint from (1), E_{mult}. RE soil temperature and moisture constraints from (6), T_{mult} and W_{mult}, respectively. Shaded bars represent L4C frozen soil classification.

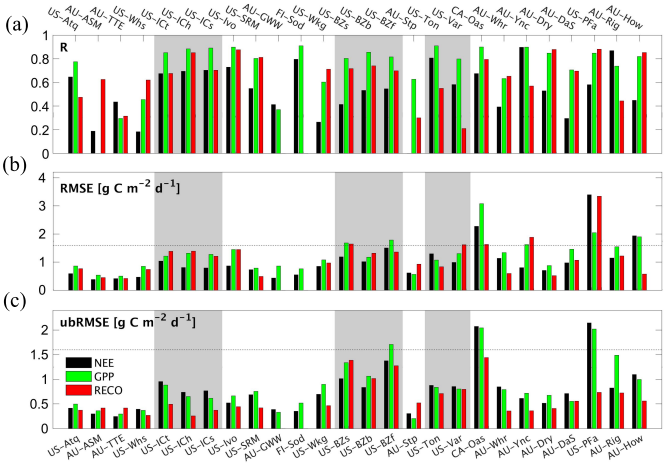

Fig. 3. CVS statistical summaries of tower observation agreement for the daily L4C Ops record including (a) Pearson's correlation (R), (b) RMSE, and (c) ubRMSE. Negative correlations (not shown) include AU-ASM (NEE) and AU-Stp (GPP). Sites AU-GWW and FI-Sod did not report RE observations. Sites sorted from left to right in order of increasing annual carbon flux magnitude from the L4C NRv4 climatology. Shaded bars indicate spatially adjacent tower sites within the same L4C 9-km grid cell. Dashed line indicates L4C NEE ubRMSE target accuracy (1.6 g·C·m^{-2}·d^{-1}).

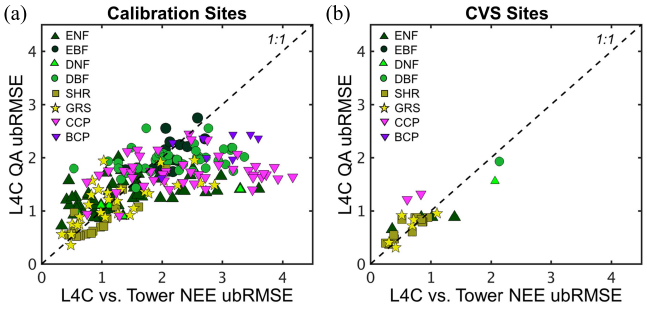

Fig. 4. L4C QA ubRMSE error estimates versus ubRMSE calculated using L4C NEE and tower site observed NEE. (a) Fitted L4C Calib average daily NEE ubRMSE (g·C·m^{-2}·d^{-1}) QA metric relative to ubRMSE calculated using NEE from calibration tower sites. (b) L4C Ops average daily NEE ubRMSE (g·C·m^{-2}·d^{-1}) QA metric relative to ubRMSE calculated using independent CVS tower NEE observations. Symbols denote dominant PFT classification of each tower location.

while NEE showed the lowest correlations relative to the tower observations. The RMSE differences were generally proportional to the size of the carbon flux, with GPP and NEE having the highest and lowest RMSE levels, respectively. NEE shows a somewhat larger though nonsignificant ($p > 0.05$) correlation increase than GPP when the L4C Ops and L4C Calib climatology results are compared, whereas RE was generally consistent between the L4C Ops and L4C Calib results. Likewise, no significant correlation skill differences were observed between L4C Ops and L4C Open Loop. Example L4C Ops time series for two tower locations with widely different climate and moisture conditions (US-Ivo and US-SRM) indicate that L4C Ops reproduces both the seasonal cycle and shorter term variability of the tower carbon flux observations (Fig. 2).

Two sites (CA-Oas and US-PFa) exceed the targeted (1.6 g·C·m^{-2}·d^{-1}) ubRMSE performance threshold for L4C Ops NEE, with respective ubRMSE differences of 2.06 and 2.13 g·C·m^{-2}·d^{-1} (Fig. 3). Two other sites (AU-ASM and AU-Stp) show negative correlations between L4C and tower observations for GPP and NEE, respectively ($R = -0.23$ and -0.19; Fig. 3). Both CA-Oas and US-PFa towers are located in productive deciduous broadleaf forests. CA-Oas is located within an aspen grove surrounded by spruce forest, so the L4C model classifies the overlying 9-km tower grid cell as ENF dominant based on the MODIS land cover inputs. The US-PFa site is surrounded by wetlands which are not identified in the MODIS PFT classification, although the L4C model classifies the 9-km tower grid cell as DBF dominant. Small negative correlations for the AU-ASM and AU-Stp sites occur because the primary growing season at these arid sites is between January and March, which falls outside of the April–December study period such that the GPP and NEE observations are near zero with little variability.

Comparison of the NEE ubRMSE QA metric against observed model and tower ubRMSE differences for the tower calibration sites shows favorable correspondence for ubRMSE ≤ 2 g·C·m^{-2}·d^{-1} [Fig. 4(a)]. However, the estimated ubRMSE QA metric shows apparent saturation and degraded

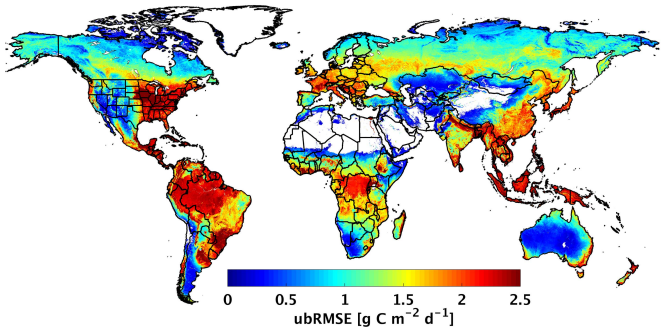

Fig. 5. Mean daily L4C Calib NEE QA ubRMSE (g·C·m^{-2}·y^{-1}) computed as the annual mean sum of squares of the daily QA ubRMSE estimates. Areas outside of the L4C model domain are denoted in white.

performance at higher error levels (above ≈2 g·C·m^{-2}·d^{-1}), especially for relatively productive ENF, DBF, CCR, and BCR cover types. Nevertheless, a similar comparison against the independent CVS observations shows favorable model correlation ($R^2 = 0.71$; $p < 0.01$), indicating that the NEE ubRMSE QA metric provides a reasonable indicator of the site-to-site variability in the L4C model accuracy [Fig. 4(b)].

The global L4C NEE QA pattern indicates that model ubRMSE accuracy tends to scale proportionally with overall ecosystem productivity (Fig. 5). The estimated ubRMSE results suggest that the targeted 1.6 g·C·m^{-2}·d^{-1} accuracy threshold for NEE is met for 66% of the global domain and 83% of the northern domain (≥45° N). The highest estimated ubRMSE occurs in relatively productive croplands, temperate deciduous forests, and tropical evergreen broadleaf forests, where the NEE ubRMSE typically exceeds 1.6 g·C·m^{-2}·d^{-1}. However, redefining estimated model uncertainty as a proportion of the estimated total carbon flux indicates that a 30% relative error (i.e., NEE ubRMSE over the sum of GPP and RE) threshold is met for 82% of the global model domain; these results indicate that the L4C product provides meaningful accuracy in many productive areas although the estimated NEE ubRMSE levels may exceed the 1.6 g·C·m^{-2}·d^{-1} threshold.

B. GOME-2 SIF Comparison

The L4C Calib GPP- and GOME-2 SIF-derived seasonal climatology results had generally consistent global patterns and mean latitudinal gradient ($R = 0.83$ globally across months and grid cells), although L4C had a somewhat longer growing season for some regions [Fig. 6(a) and (b)]. Poleward of 35° N, GOME-2 SIF, and GPP closely agree for growing season onset, peak, and duration. From 20° N to 35° N, the L4C results show a longer and more persistent growing season than GOME-2 SIF, with increasing difference toward the tropical southern portion of this region. From 5° S to 15° N, the L4C results had peak growing season productivity during August and September, while the GOME-2 SIF results indicate a seasonal productivity minimum during this period. Poleward of 5° S, the L4C GPP, and GOME-2 SIF results show similar peak timing and seasonality, although L4C showed a slightly longer growing season in the 35° S–45° N region.

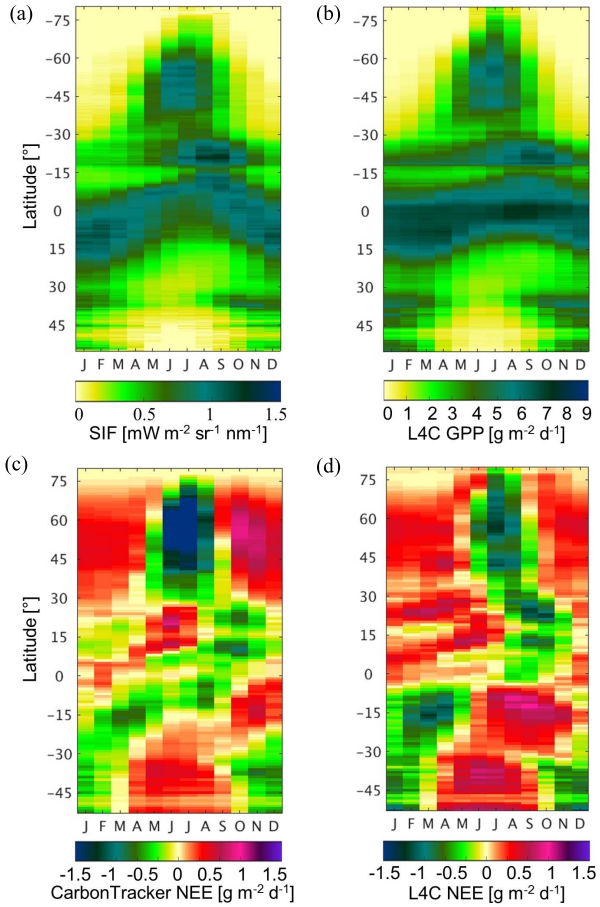

Fig. 6. Monthly climatological (2000–2012) zonal averages for (a) GOME-2 SIF, (b) L4C Calib GPP, (c) CarbonTracker (CT2013B), and (d) L4C Calib NEE. CarbonTracker and L4C Calib NEE assigned differing color scaling to show variability (see Section II-D).

C. CarbonTracker Bioflux Comparison

The L4C Calib NEE and CarbonTracker biological fluxes had a coherent climatology for all latitudes and similar latitudinal gradients ($R = 0.60$ globally across months and grid cells). However, the timing, length and depth of the estimated CO_2 uptake periods are most consistent poleward of 30° S with notable L4C and CarbonTracker differences elsewhere [Fig 6(c) and (d)]. Poleward of 30° N, the CarbonTracker results indicate earlier CO_2 uptake onset, earlier peak uptake, and larger fall CO_2 release relative to L4C NEE. Between 0° and 30° N, CarbonTracker showed greater CO_2 release prior to CO_2 uptake onset. Between 0° and 30° S, the L4C Calib NEE results showed a longer and deeper CO_2 uptake period directly followed by peak CO_2 release from August to September, whereas CarbonTracker indicated a relatively short and shallow uptake period followed by peak CO_2 release from October to November.

D. SOC Comparison

The L4C Calib results generally reproduced the global SOC patterns when compared to the IGBP-DIS and NCSCD soil inventories, including relatively higher SOC stocks in the

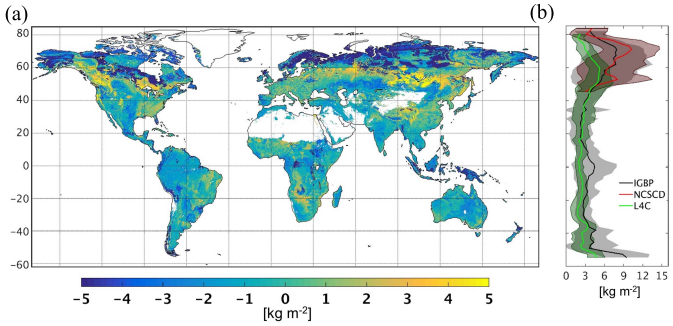

Fig. 7. Comparison of L4C Calib initialized SOC (representing <10 cm depth) to global and high-latitude inventory-based SOC (depth adjusted to <10 cm depth) data sets including (a) differences between L4C initialized steady-state SOC and IGBP-DIS (i.e., L4C−IGBP) and (b) zonal mean SOC for L4C, NCSCD (>50 N only), and IGBP-DIS. Nonvegetated areas outside of the L4C model domain in (a) are denoted in white. Shading in (b) indicates ± standard deviation for latitude zone.

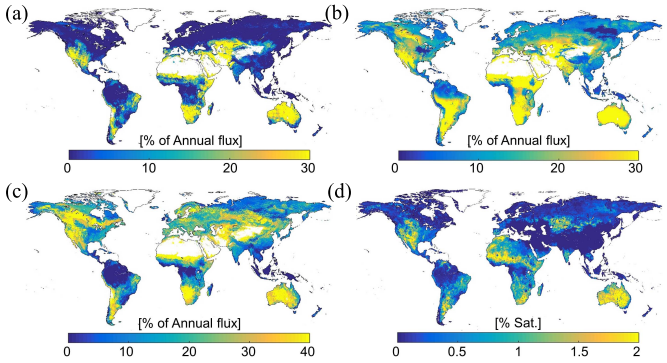

Fig. 8. Global metrics indicating the impact of soil moisture sensitivity analysis and operational SMAP observations on L4C Calib flux climatology fields. Percentage decrease in annual (a) GPP computed using SMRZ versus without SMRZ, (b) GPP computed using VPD versus without VPD, and (c) RH computed using SMSF versus without SMSF. (d) Standard deviation of the L4SM SMSF analysis increment (data assimilation update minus model forecast) in percent saturation units. Nonvegetated areas outside of the L4C model domain in (a)–(c) are denoted in white.

high northern latitudes relative to the mid-latitudes (Fig. 7). However, there were notable differences. In tropical and arctic regions, L4C SOC stocks were somewhat less than indicated by the IGBP-DIS and NCSCD inventories. Throughout many portions of the circumpolar boreal latitudes, L4C SOC stocks were greater than those in the IGBP-DIS and NCSCD inventories. In general, the L4C SOC distribution peaked in the boreal forest zone (50°–60° N), whereas the SOC distributions from IGBP and NCSCD peaked near 65°–70° N. The low bias of L4C SOC l relative to IGBP in boreal and artic regions (50°–70° N) may be related to the prevalent spatial distribution of extensive wetlands characterized by thick organic sediments which contain old soils and wetland characteristics not represented in L4C or Catchment model [57]. Although the inventory records showed a similar mean SOC polar latitudinal gradients, considerable differences in SOC spatial patterns also occur between the IGBP-DIS and NCSCD records. The NCSCD record may be more accurate since it contains additional ground samples, and includes estimation focused on high-latitude conditions particularly including wetland soil types [57].

E. L4C Model Sensitivity Analysis

The L4C Calib climatological model sensitivity analysis indicated that SMRZ had substantial impact on annual GPP (≥30% annual difference) over approximately 12% of the global model domain and some impact (≥5% annual difference) over 38% of the global domain. These areas of impact are particularly over drier climate regions [Fig. 8(a)]. The GPP results reflect the impact of soil moisture on estimated productivity in addition to contributions from model FPAR and VPD inputs, which also correlate with moisture availability. Atmospheric VPD has relatively more widespread impact on estimated GPP than SMRZ, with notable importance for tropical "dry" (seasonal) forests including Africa, semiarid, and arid Australia and also for boreal forests, particularly in North America [Fig. 8(b)]. Moisture constraints from SMRZ and VPD show little impact on GPP for broadleaf crops, deciduous needleleaf forests, and tropical forests (with the exception of central Africa), although the L4C flux tower calibration data set lacked DNF tower site representation.

The impact of SMSF on RH is more widespread than the impact of SMRZ on GPP [Fig. 8(a) and (c)]. These results are consistent with the larger number of environmental controls influencing the L4C GPP (and RA) calculations, whereas only SMSF and soil temperature are used as the primary environmental controls on model estimated SOC decomposition and RH. SMSF has a little impact on RH in equatorial tropical forests which lack a pronounced wet season.

The standard deviation of the L4SM soil moisture analysis increments indicates that SMAP observations most impact L4SM in arid and semiarid regions, which generally align with higher L4C soil moisture sensitivity [Fig. 8(a), (c), and (d)]. However, L4SM SMSF analysis increment variability (i.e., data assimilated SMSF versus forecast SMSF) is relatively small compared to overall soil moisture variance because the L4SM data assimilation affects only TB anomalies and therefore mostly affects subseasonal soil moisture variations. Consequently, the largest differences between L4C Ops and L4C Open-Loop differences occur in arid regions [Fig. 9(b) and (d)] and align with regions of high L4C Calib interannual variability (Fig. 9). GPP shows a relatively larger soil moisture sensitivity and higher interannual variability than NEE because the GPP and RH responses partially offset each other in the residual NEE term [Fig. 9(a) and (c)]. Although the L4C NEE response patterns were generally similar to GPP and of lower magnitude, the circumpolar boreal forest was a notable exception where RH influenced the NEE sensitivity pattern [Fig. 9(d)].

IV. Discussion

A. Uncertainty Evaluation

The CVS comparisons indicate that the L4C Ops results capture daily-to-seasonal variations and regional patterns in tower observed terrestrial carbon fluxes spanning a broad range of global climate and vegetation conditions

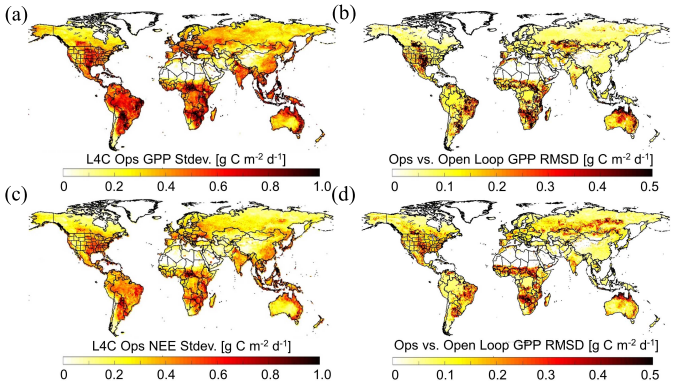

Fig. 9. Comparison of L4C Calib interannual anomaly variability with SMAP impact as measured by difference variance between L4C Ops and L4C Open-Loop simulations. Shown are L4C Calib interannual anomaly standard deviations (for 2000–2012) for (a) GPP and (c) NEE compared with L4C Ops versus L4C Open-Loop root-mean-square difference (from March 31, 2015 to December 31, 2015) and for (b) GPP and (d) NEE. Variances expressed in average daily carbon flux units ($g{\cdot}C{\cdot}m^{-2}{\cdot}d^{-1}$). Nonvegetated areas outside of the L4C model domain are denoted in white.

(Table IV and Figs. 1 and 2). The L4C Ops-derived GPP seasonality was generally proportional to RE, resulting in a relatively lower NEE seasonality (Fig. 3). The NEE generally had lower RMSE than GPP or RE relative to the tower observations because of smaller characteristic magnitude of the residual NEE flux (Table V). Likewise, higher correlations between the tower observations and L4C results for GPP and RE relative to NEE were largely due to the smaller seasonal cycle of NEE rather than actual model skill differences (Fig. 3). However, somewhat lower correlations between measured and modeled RE and NEE relative to GPP were partially impacted by model SOC mismatches relative to local site conditions which affect both L4C-derived carbon fluxes and estimated error (ubRMSE) variance. Larger-than-expected model carbon flux ubRMSE and negative correlations with tower observations for some CVS locations were attributed to land cover (PFT) differences between the local tower footprint and the MODIS 1-km land cover map used to define PFT heterogeneity in the L4C model, or to the limited (April–December 2015) study period that missed the primary growing season for some sites (AU-ASM and AU-Stp). More productive tower sites (CA-Oas and US-PFa) also had relatively larger carbon fluxes and associated ubRMSE levels, although relative model error, expressed as a proportion of the total estimated carbon flux magnitude, indicated meaningful model accuracy across a broad range of global vegetation, productivity, and climate conditions (Fig. 3).

The NEE ubRMSE QA results for L4C Ops and L4C Calib simulations indicate a general increase of model error with estimated carbon flux magnitude over the global domain (Figs. 4 and 5). However, the model calibration results indicate that the explanatory power of the NEE QA metric saturates for higher ubRMSE levels beyond ≈ 2 $g{\cdot}C{\cdot}m^{-2}{\cdot}d^{-1}$, which is generally characteristic of productive croplands and forests [Fig. 4(a)]. Croplands often contain diverse crop types, riparian areas, and fallow fields, whereas forestland is often interspersed with cropland and pasture, and composed of different age classes and recovery stages from land-use change, burning, or harvesting. The resulting subgrid spatial heterogeneity in vegetation and soil conditions will tend to increase both random and bias errors in estimated carbon fluxes, leading to degraded ubRMSE accuracy. Other factors such as subgrid PFT spatial heterogeneity and disturbance history likely dominated overall model uncertainty for such locations. Despite these limitations, the CVS results indicate that the L4C Ops ubRMSE QA metric provides a relatively robust measure of model NEE uncertainty [Fig. 4(b)]. Previous studies using similar satellite data-driven LUE models [59] indicate that model input uncertainty is a major source of model error (up to 30%), whereas the L4C QA metric provides a daily estimate of the aggregate effects of model inputs and assumptions on product accuracy.

B. Evaluation Relative to Other Global Data sets

The L4C Calib- and CarbonTracker-derived NEE climatologies were generally consistent over the global domain [Fig. 6(c) and (d)]. However, some areas showed different NEE spatial and temporal patterns, which may reflect model differences in seasonal litterfall regimes. Model differences in underlying climatic drivers and control factors affecting GPP and RE also impact these patterns but likely to a lesser extent. The CASA land model used in CarbonTracker has a prescribed litterfall phenology [60] and provides the estimated monthly NEE priors used in the CarbonTracker inversion; CASA model NEE priors are responsible for most of the CarbonTracker subcontinental spatial variability. Unlike CASA, the L4C model has a daily time step and evenly distributes litterfall throughout the year. (That is, $L_{\text{fall}}-$ in (6) and (7) is constant for all t.) Since NEE peak uptake is mainly driven by GPP, the relatively early CarbonTracker uptake onset and seasonal peak for northern ($>40°$ N) areas are at odds with both GOME-2 SIF and L4C Calib GPP climatologies which suggest that the ecosystem carbon uptake onset and peak should occur later [Fig 6(a) and (b)]. Nevertheless, L4C Calib carbon flux patterns generally align with typical GPP and NEE seasonal trends indicated from the GOME-2 SIF and CarbonTracker NEE benchmark data sets.

Changes in NEE trends over decades and longer will result in measurable changes to SOC stocks. Although comparisons of dynamic models, such as L4C, with inventory-based SOC maps are problematic, understanding spatial differences potentially provides insight regarding model and sampling uncertainty, and driving processes. The relative L4C underestimation of SOC in the high latitudes is attributable to a lack of detailed information on wetlands and peatlands (Fig. 7). The L4C Calib results show peak SOC accumulation in the boreal latitudes because of the combination of moderate litterfall and cold conditions favoring SOC accumulation. Matching the larger SOC levels indicated from the soil inventory data would therefore require lengthening of L4C effective SOC turnover times for boreal and arctic latitudes. The apparent difference in L4C derived versus effective turnover times may reflect the prevalence of boreal and tundra wetlands and peatlands, and associated anaerobic soil conditions, or differences in SOC quality [45] that may not be effectively represented by the model inputs and assumptions. Although SOC may provide

some insight for improving L4C RH estimates, the potential for improvement is ultimately limited by several factors. SOC development generally occurs over long periods (i.e., thousands of years or more) subject to changing climate and ecological conditions, so L4C model-based SOC estimates derived from recent satellite and meteorological records are expected to diverge from soil inventory records. Wetlands and peatlands accumulate large SOC stocks, and are common in boreal, arctic, and equatorial (tropical) biomes where a relatively large model and inventory discrepancies were found. These areas are not well represented by the global flux tower network, and there is little available flux information for robust L4C calibration of global wetland dynamics. Furthermore, SOC characteristically shows large spatial heterogeneity in wetland regions influenced by surface and sub-SMSF dynamics that exist beneath the resolution of coarser scale SMAP observations and model derived products (L4C and L4SM). New fine-scale radar-based remote-sensing approaches for estimating soil carbon indicate approximately 25% lower SOC in some arctic areas than indicated from NSCDC inventory records [61]. Considering such mismatches, inventory-based SOC assessments may benefit from the comparison of climate-induced dynamics and spatial covariance metrics provided by the L4C product and other remote-sensing data sets.

C. Value of Soil Moisture and SMAP Observations

The L4C Calib model sensitivity analysis indicated the widespread impact of soil moisture on terrestrial carbon fluxes (Fig. 8). SMRZ primarily impacts GPP in arid regions, whereas SMSF has a more widespread impact on RH. SMRZ is used with VPD inputs to represent both soil water supply and atmospheric moisture demand controls on GPP. SMRZ provides an additional impact on GPP extending beyond VPD controls over drier climates of the global domain, where the SMAP observations have generally greater impact on the GEOS-5 land model assimilation used to derive the L4SM soil moisture and temperature inputs. The impact of SMSF on RH was more widespread than that of SMRZ and GPP because SMSF provides the sole moisture constraint to the model RH calculations. RH also has an exponential dependence on temperature in the L4C model so that dry conditions have a relatively greater impact on respiration when co-occurring with high temperatures. SMSF has generally larger dynamic variability than SMRZ such that RH shows larger daily variability in response to rapid wetting/drying of the surface soil layer.

Other recent studies have highlighted the importance of arid regions for controlling interannual variability of the global land carbon flux [2]–[4]. This global variability is strongly influenced by periodic wet and dry (drought) cycles, associated fire events, and concomitant effects on vegetation growth and NEE in dryland ecosystems, including grasslands, shrublands, and savannahs [4]. In arid and seasonally arid regions, RE rapidly responds to rainfall (i.e., the so-called "Birch effect" [62]) and in both arid and nonarid ecosystems, root exudates from trees and shrubs can provide "priming" effects increasing RE after soil wetting [63]. Both effects underscore the importance of daily soil moisture for modeling RE and NEE fluxes. In contrast, carbon flux spatiotemporal variability in more humid biomes, especially forests, may be relatively more impacted by the interaction of drought with disturbance (fire, harvesting, etc.) and recovery processes, which are not explicitly modeled in the current L4C Ops product. Water logged and saturated soils can inhibit RH by decreasing oxygen availability and causing anaerobic conditions [64]; however, inclusion of an inverse-parabolic RH response curve degraded the PFT-specific L4C calibration fit in relation to the global tower calibration sites used in this study. The lack of an apparent anaerobic response may be due one or more factors including a general lack of wetland representation and flooding in the FLUXNET tower site record used for model calibration; the relatively coarse (9 km) resolution L4SM information used to define model soil moisture conditions may not effectively capture saturated or ephemerally flooded conditions, while anaerobic conditions may also be partially offset by plant root-mediated oxygen transport [65]. Lack of anaerobic response also likely plays a role in L4C SOC low bias arctic, boreal, and some tropical wetland locations (Fig. 7; Section IV-B.).

The full global range of vegetation and climate conditions, including climate extremes, disturbance, and recovery, are generally under-sampled by the available flux tower network [65], [48]. Since tower data were used to calibrate the L4C model, the above global soil moisture sensitivity analysis is biased to the existing tower network [9], [66]. The relatively short time period used in this study (March 31, 2015 to December 31, 2015) restricts a more comprehensive soil moisture sensitivity assessment because many locations (e.g., tropical evergreen broadleaf forests) may only respond to extreme events that that occur infrequently and may not be represented in the relatively recent (2001–2012) MODIS and NRv4 records used to derive the L4C simulations. These types of sampling biases affect all L4C results in this study, have been noted by other global studies, and are largely unavoidable [66], [67]. Additionally, methods used to partition GPP and RE components of NEE from tower eddy covariance CO_2 flux measurements are modeled following various assumptions and therefore do not truly represent "observations [50]." Each tower's effective spatial footprint changes with wind direction and may be inconsistent with the associated 1-km L4C modeling pixel. Effective SOC storage mismatches between the L4C model steady-state initialization cause further uncertainty. The use of model cross-comparisons and rescaling with alternative observation benchmarks such as GOME-2 SIF and CarbonTracker provide for additional model validation, although these somewhat indirect comparisons can also be difficult to interpret.

Our results indicate only a relatively small benefit of SMAP observations on the L4C calculations based on the limited data record examined in this study. The accuracy and performance of L4C Ops were on par with the L4C Open Loop and only marginally better than the L4C Calib climatology from the CVS results (Section III A; Table V). The results are also impacted by the inclusion of CVS locations where low soil moisture is not generally limiting to ecosystem carbon fluxes. The relatively early mission phase and associated short CVS time record ($<$1 full year) currently limits capabilities for a more robust assessment of the impact of SMAP observations

on the L4C model skill relative to flux towers. Moreover, the microwave emission model used for assimilating SMAP observations and L4SM production was necessarily calibrated using SMOS data during the SMAP mission prelaunch phase, which limits which limits the use of SMAP TB observations in the L4SM system to the areas where SMOS is not impacted by radio frequency interference. Similarly, the L4C model was necessarily calibrated using NRv4 inputs (L4C Calib), which may dampen or bias results when confronted with SMAP informed L4SM soil moisture and temperature inputs used in the L4C Ops product. Such relative biases are particularly common for soil moisture data sets from both model and remote-sensing sources [31]–[33], and perhaps more pervasive than for other meteorological fields such as air temperature and humidity [68]. This is because the global soil moisture fields have been historically poorly observed, and because soil moisture has generally large characteristic heterogeneity leaving the true global soil moisture field unknown and absolute biases indeterminate. Such biases are problematic for L4C (and all such models [31]), especially if the magnitude of soil moisture bias exceeds its temporal variability, because these biases can lead to model calibration errors affecting the PFT-specific soil moisture constraint curves.

Despite the seemingly small benefit of SMAP observations at CVS sites, L4C interannual variability is well aligned with regions where SMAP provides the most information in the L4SM data assimilation (Figs. 8 and 9). These regions mostly include arid and semiarid regions, and also extend to a few boreal locations. Furthermore, these regions also coincide with where L4C is most sensitive to soil moisture. Taken together, these results indicate that SMAP provides its most useable information where soil moisture limitations control GPP and NEE interannual variability and where L4C is most sensitive to soil moisture limitation. This indicates the potential of microwave-derived global soil moisture information to estimate terrestrial CO_2 fluxes, with larger impacts in drier climates and areas with less vegetation cover where SMAP observations have greater soil moisture sensitivity and associated impact on land model data assimilation soil moisture estimates. Planned model calibration refinements and a continuing SMAP operational record are expected to lead to further improvements in L4C global accuracy and performance as indicated by CVS locations and global data set intercomparisons.

V. Conclusion

The SMAP L4C product provides consistent, operational global daily estimates of ecosystem-atmosphere carbon fluxes, surface SOC stocks, and their underlying environmental controls. Our initial global assessment using several independent observation benchmarks indicates that the L4C model accuracy and performance is consistent with product design specifications and target accuracy requirements, and that the L4C product is suitable for a range of science investigations, including drought-related impacts on vegetation growth and the terrestrial carbon cycle. The L4C product provides a new tool for monitoring global land carbon dynamics informed by model data assimilation of SMAP satellite observations with enhanced L-band microwave sensitivity to soil moisture and thermal conditions.

The L4C product suite includes internally consistent estimates of NEE, component carbon fluxes (GPP and RH), and surface SOC stocks. Additional product variables include underlying environmental control factors influencing GPP and RH, and NEE ubRMSE QA metrics that provide enhanced diagnostic capabilities for analysis and attribution of estimated carbon fluxes and driving processes. The L4C model outputs are derived at a daily time step and 1-km resolution, capturing weather-related daily variability at the level of a tower carbon flux measurement footprint.

The results of this study document the L4C model accuracy relative to independent tower carbon flux observations and indicate that SMAP observations are most useful where soil moisture strongly controls land CO_2 flux dynamics and variability. The L4C results were also verified against other available carbon observation benchmarks including satellite-based SIF from GOME-2, used as a surrogate for GPP, atmosphere transport model inversion-constrained NEE estimates from CarbonTracker, and global soil carbon inventory records. These results indicate that L4C performance is within the targeted accuracy threshold for NEE (ubRMSE $\leq$ 1.6 $g{\cdot}C{\cdot}m^{-2}{\cdot}d^{-1}$ or 30 $g{\cdot}C{\cdot}m^{-2}{\cdot}y^{-1}$) over approximately 66% of the global domain, and with larger absolute error but still meaningful accuracy (relative error $\leq$ 30%) over 82% of the global domain. The L4C product performance for estimated carbon fluxes is generally commensurate with the level of uncertainty associated with *in situ* tower carbon flux observations.

Model comparisons with CarbonTracker indicate that the L4C results contain potentially new information for informing global carbon flux inversions, including providing direct links between NEE variability and underlying soil moisture and thermal constraints to ecosystem productivity, respiration, and terrestrial carbon storage processes. Model sensitivity and variability analyses indicated that microwave-based soil moisture potentially add useful new information for improving the estimation of terrestrial carbon fluxes and underlying environmental controls, especially for arid and semi-arid climate regions, because such regions are where SMAP observations inform the L4SM data assimilation and where water availability largely controls land CO_2 flux. Although benefits of using SMAP data are not yet discernable relative to the short record of CVS flux tower observations, the L4SM and L4C records will continue to benefit from continuing SMAP operations and ongoing sensor and model calibration refinements which will likely improve detectability of SMAP impact as a longer record becomes available. The L4C product provides the means for addressing mission carbon cycle science objectives to improve understanding of the purported missing carbon sink on land, and link terrestrial water and carbon cycles.

Acknowledgment

Computational resources were provided by the NASA High-End Computing Program through the NASA Center for Climate Simulation. The authors would like to thank the SMAP L4C Calibration and Validation flux tower partners

and La Thuile synthesis site investigators for the contribution of flux tower data. They would like to thank the SMAP L4C Cal/Val partners who contributed data but did not co-author: M. Aurela (Finnish Meteorological Institute, Helsinki, Finland), D. Baldocchi (University of California, Berkley, CA, USA), J. Beringer (University of Western Australia, Crawley WA, Australia), W. Oechel (San Diego State University, San Diego, CA, USA), and H. Wheater (University of Saskatchewan, Saskatoon, SK, Canada). The La Thuile synthesis data set includes eddy covariance data acquired by the FLUXNET community and in particular by the following networks: AmeriFlux (U.S. Department of Energy, Biological and Environmental Research, Terrestrial Carbon Program (DE-FG02-04ER63917 and DE-FG02-04ER63911), AfriFlux, AsiaFlux, CarboAfrica, CarboEuropeIP, CarboItaly, CarboMont, ChinaFlux, Fluxnet-Canada (supported by CFCAS, NSERC, BIOCAP, Environment Canada, and NRCan), GreenGrass, KoFlux, LBA, NECC, OzFlux, TCOS-Siberia, and USCCC. They would also like to thank CarboEuropeIP, FAO-GTOS-TCO, iLEAPS, the Max Planck Institute for Biogeochemistry, National Science Foundation, the University of Tuscia, the Université Laval, Environment Canada, and the U.S. Department of Energy, for the financial support to the eddy covariance data harmonization, and the Berkeley Water Center, the Lawrence Berkeley National Laboratory, Microsoft Research eScience, the Oak Ridge National Laboratory, the University of California, Berkeley, and the University of Virginia, for the database development and technical support, OzFlux and the Australia Terrestrial Ecosystem Research Network (http://www.tern.org.au) for the support with collection and archiving of Australian flux data, and D. Baldocchi and J. Beringer for their comments and discussions which helped improve this manuscript.

REFERENCES

[1] J. G. Canadell *et al.*, "Contributions to accelerating atmospheric CO_2 growth from economic activity, carbon intensity, and efficiency of natural sinks," *Proc. Nat. Acad. Sci. USA*, vol. 104, no. 47, pp. 18866–18870, 2007.

[2] A. Ahlström *et al.*, "The dominant role of semi-arid ecosystems in the trend and variability of the land CO_2 sink," *Science*, vol. 348, no. 6237, pp. 895–899, 2015.

[3] J. Cleverly *et al.*, "The importance of interacting climate modes on Australia's contribution to global carbon cycle extremes," *Sci. Rep.*, vol. 6, Nov. 2016, Art. no. 23113.

[4] B. Poulter *et al.*, "Contribution of semi-arid ecosystems to interannual variability of the global carbon cycle," *Nature*, vol. 509, pp. 600–603, May 2014.

[5] M. Zhao and S. W. Running, "Drought-induced reduction in global terrestrial net primary production from 2000 through 2009," *Science*, vol. 329, no. 5994, pp. 940–943, 2010.

[6] Y. Y. Liu *et al.*, "Recent reversal in loss of global terrestrial biomass," *Nature Climate Change*, vol. 5, no. 5, pp. 470–474, 2015.

[7] D. Entekhabi *et al.* (2014). "Soil moisture active passive (SMAP) mission handbook," California Inst. Technol. Jet Propulsion Lab., Pasadena, CA, USA, Tech. Rep. 180. [Online]. Available: https://smap.jpl.nasa.gov/system/internal_resources/details/original/178_SMAP_Handbook_FINAL_1_JULY_2014_Web.pdf

[8] D. Entekhabi *et al.*, "The soil moisture active and passive (SMAP) mission," *Proc. IEEE*, vol. 98, no. 5, pp. 704–716, May 2010.

[9] D. Schimel *et al.*, "Observing terrestrial ecosystems and the carbon cycle from space," *Global Change Biol.*, vol. 21, no. 5, pp. 1762–1766, 2015.

[10] R. H. Reichle *et al.*, "Assessment of the SMAP level 4 surface and root zone soil moisture product using *in situ* measurements," *J. Hydrometeorol.*, to be published, doi: 10.1175/JHM-D-17-0063.1.

[11] R. H. Reichle, G. J. M. De Lannoy, R. D. Koster, W. T. Crow, and J. S. Kimball. (2016). "SMAP L4 9-km EASE grid surface and root zone soil moisture geophysical data, version 2," NASA Nat. Snow Ice Data Center Distrib. Active Arch. Center, Boulder, CO, USA, Dataset, Accessed on Jan. 5, 2016. [Online]. Available: http://dx.doi.org/10.5067/YK70EPDHNF0L

[12] R. H. Reichle, G. J. M. De Lannoy, R. D. Koster, W. T. Crow, and J. S. Kimball. (2016). "SMAP L4 9-km EASE grid surface and root zone soil moisture analysis update, version 2," NASA Nat. Snow Ice Data Center Distrib. Active Arch. Center, Boulder, CO, USA, Dataset, Accessed on Jan. 5, 2016. [Online]. Available: http://dx.doi.org/10.5067/JJY2V0GJNFRZ

[13] R. H. Reichle, G. J. M. De Lannoy, R. D. Koster, W. T. Crow, and J. S. Kimball. (2016). "SMAP L4 9-km EASE grid surface and root zone soil land model constants, version 2," NASA Nat. Snow Ice Data Center Distrib. Active Arch. Center, Boulder, CO, USA, Tech. Rep., accessed on Jan. 5, 2016. [Online]. Available: http://dx.doi.org/10.5067/VBRUC1AFRQ22

[14] R. H. Reichle *et al.*, "Soil moisture active passive mission level 4 surface and root zone soil moisture (L4_SM) product specification document. GMAO Office Note No. 10 (Version 1.4)," Goddard Space Flight Center, Greenbelt, MD, USA, Tech. Rep., Oct. 2015. [Online]. Available: https://gmao.gsfc.nasa.gov/pubs/docs/Reichle789.pdf

[15] J. S. Kimball, L. A. Jones, J. Glassy, and R. H. Reichle. (2016). "SMAP L4 global daily 9-km carbon net ecosystem exchange, version 2," NASA Nat. Snow Ice Data Center Distrib. Active Arch. Center, Boulder, CO, USA, Dataset, Accessed on Jan. 5, 2016. [Online]. Available: http://dx.doi.org/10.5067/UBKO5zUI715V

[16] J. Glassy *et al.* (Apr. 2016). "Soil moisture active passive (SMAP) mission level 4 carbon (L4_C) product specification document," GMAO Office Note No. 11 (Version 2.0), Goddard Space Flight Center, Greenbelt, MD, USA, Tech. Rep. [Online]. Available: https://gmao.gsfc.nasa.gov/pubs/docs/Glassy850.pdf

[17] C. S. Potter *et al.*, "Terrestrial ecosystem production: A process model based on global satellite and surface data," *Global Biogeochem. Cycles*, vol. 7, no. 4, pp. 811–841, 1993.

[18] F. S. Chapin, P. A. Matson, and H. A. Mooney, "Terrestrial decomposition," in *Principles Terrestrial Ecosystem Ecology*. New York, NY, USA: Springer, 2002, ch. 7, pp. 151–175.

[19] W. J. Parton, D. S. Schimel, C. V. Cole, and D. S. Ojima, "Analysis of factors controlling soil organic matter levels in Great Plains grasslands," *Soil Sci. Amer. J.*, vol. 51, pp. 1173–1179, Sep. 1987.

[20] E. A. Davidson, K. E. Savage, S. E. Trumbore, and W. Borken, "Vertical partitioning of CO_2 production within a temperate forest soil," *Global Change Biol.*, vol. 12, no. 6, pp. 944–956, 2006.

[21] Y. Ryu *et al.*, "Integration of MODIS land and atmosphere products with a coupled-process model to estimate gross primary productivity and evapotranspiration from 1 km to global scales," *Global Biogeochem. Cycles*, vol. 25, no. 4, p. B4017, 2011.

[22] K. D. Kanniah, J. Beringer, L. B. Hutley, N. J. Tapper, and X. Zhu, "Evaluation of collections 4 and 5 of the MODIS gross primary productivity product and algorithm improvement at a tropical savanna site in northern Australia," *Remote Sens. Environ.*, vol. 113, no. 9, pp. 1808–1822, 2009.

[23] S. W. Running, R. R. Nemani, F. A. Heinsch, M. Zhao, M. Reeves, and H. Hashimoto, "A continuous satellite-derived measure of global terrestrial primary production," *Bioscience*, vol. 54, no. 6, pp. 547–560, 2004.

[24] W. Peters *et al.*, "An atmospheric perspective on North American carbon dioxide exchange: CarbonTracker," *Proc. Nat. Acad. Sci. USA*, vol. 104, no. 48, pp. 18925–18930, 2007.

[25] J. S. Kimball, L. A. Jones, J. Glassy, and R. Reichle. (2014). "SMAP algorithm theoretical basis document, release A: L4 carbon product," Jet Propulsion Lab., Pasadena, CA, USA, Tech. Rep. JPL D-66484. [Online]. Available: https://nsidc.org/data/docs/daac/smap/sp_l4_cmdl/pdfs/271_L4_C_RevA_web.pdf

[26] M. J. Brodzik, B. Billingsley, T. Haran, B. Raup, and M. H. Savoie, "*EASE-Grid 2.0:* Incremental but significant improvements for earth-gridded data sets," *ISPRS Int. J. Geo-Inf.*, vol. 1, pp. 32–45, Sep. 2012.

[27] J. S. Kimball *et al.* (Apr. 2016) "Soil moisture active passive mission L4_C data product asssessment (version 2 validated release)," GMAO Office Note No. 13, NASA Goddard Space Flight Center, Greenbelt, MD, USA. [Online]. Available: https://ntrs.nasa.gov/archive/nasa/casi.ntrs.nasa.gov/20160008108.pdf

[28] R. H. Reichle *et al.* (Apr. 2016). "Soil moisture active passive mission L4_SM data product assessment (version 2 validated release)," GMAO Office Note No. 12, Goddard Space Flight Center, Greenbelt, MD, USA. [Online]. Available: https://ntrs.nasa.gov/archive/nasa/casi.ntrs.nasa.gov/20160008109.pdf

[29] M. M. Rienecker *et al.*, "MERRA: NASA's modern-era retrospective analysis for research and applications," *J. Climate*, vol. 24, pp. 3624–3648, Apr. 2011.

[30] R. H. Reichle, R. D. Koster, G. J. M. De Lannoy, W. T. Crow, and J. S. Kimball. (2014). "SMAP algorithm theoretical basis document: L4 surface and root-zone soil moisture product," Jet Propulsion Lab., Pasadena, CA, USA, Tech. Rep. JPL D-66483. [Online]. Available: http://nsidc.org/sites/nsidc.org/files/files/272_L4_SM_RevA_web.pdf

[31] R. D. Koster, Z. Guo, R. Yang, P. A. Dirmeyer, K. Mitchell, and M. J. Puma, "On the nature of soil moisture in land surface models," *J. Climate*, vol. 22, pp. 4322–4335, Sep. 2009.

[32] P. A. Dirmeyer *et al.*, "Confronting weather and climate models with observational data from soil moisture networks over the United States," *J. Hydrometeorol.*, vol. 17, pp. 1049–1067, Sep. 2016.

[33] R. H. Reichle and R. D. Koster, "Bias reduction in short records of satellite soil moisture," *Geophys. Res. Lett.*, vol. 31, no. 19, pp. 1–4, 2004.

[34] G. J. M. De Lannoy and R. H. Reichle, "Global assimilation of multiangle and multipolarization SMOS brightness temperature observations into the GEOS-5 catchment land surface model for soil moisture estimation," *J. Hydrometeorol.*, vol. 17, no. 2, pp. 669–691, 2016, doi: 10.1175/JHM-D-15-0037.1.

[35] G. J. M. De Lannoy, R. H. Reichle, and V. R. N. Pauwels, "Global calibration of the GEOS-5 L-band microwave radiative transfer model over nonfrozen land using SMOS observations," *J. Hydrometeorol.*, vol. 14, pp. 765–785, Sep. 2013.

[36] R. Luchessi. (2013, June). "File specification for GEOS-5 FP (Forward Processing)," GMAO Office Note No. 4 (Version 1), NASA Goddard Space Flight Center, Greenbelt, MD, USA. [Online]. Available: https://ntrs.nasa.gov/archive/nasa/casi.ntrs.nasa.gov/20150001437.pdf

[37] M. Friedl *et al.*, "MODIS collection 5 global land cover: Algorithm refinements and characterization of new datasets," *Remote Sens. Environ.*, vol. 114, no. 1, pp. 168–182, 2010.

[38] Y. Knyazikhin *et al.*, "MODIS leaf area index (LAI) and fraction of photosynthetically active radiation absorbed by vegetation (FPAR) product (MOD15) algorithm theoretical basis document (Version 4.0)," NASA Goddard Space Flight Center (GSFC), Greenbelt, MD, USA, Tech. Rep., 1999. [Online]. Available: https://modis.gsfc.nasa.gov/data/atbd/atbd_mod15.pdf

[39] R. Whitley, B. Medlyn, M. Zeppel, C. Macinnis-Ng, and D. Eamus, "Comparing the Penman–Monteith equation and a modified Jarvis–Stewart model with an artificial neural network to estimate stand-scale transpiration and canopy conductance," *J. Hydrol.*, vol. 373, nos. 1–2, pp. 256–266, 2009.

[40] J. L. Monteith and C. J. Moss, "Climate and the efficiency of crop production in Britain [and discussion]," *Philos. Trans. Roy. Soc. London A, Math. Phys. Sci.*, vol. B281, no. 980, pp. 277–294, 1977.

[41] S. D. Prince and S. N. Goward, "Global primary production: A remote sensing approach," *J. Biogeogr.*, vol. 22, nos. 4–5, pp. 815–835, 1995.

[42] J. S. Kimball, L. A. Jones, K. Zhang, F. A. Heinsch, K. C. McDonald, and W. C. Oechel, "A satellite approach to estimate land–atmosphere CO_2 exchange for boreal and arctic biomes using MODIS and AMSR-E," *IEEE Trans. Geosci. Remote Sens.*, vol. 47, no. 2, pp. 569–587, Feb. 2009.

[43] X. Xiao, C. Jin, and J. Dong, "Gross primary production of terrestrial vegetation," in *Biophysical Applications of Satellite Remote Sensing*, J. M. Hanes, Ed. Berlin, Germany: Springer-Verlag, 2014, pp. 127–147.

[44] R. Waring, J. J. Landsberg, and M. Williams, "Net primary production of forests: A constant fraction of gross primary production?" *Tree Physiol.*, vol. 18, no. 2, pp. 129–134, 1998.

[45] T. Ise and P. R. Moorcroft, "The global-scale temperature and moisture dependencies of soil organic carbon decomposition: An analysis using a mechanistic decomposition model," *Biogeochemistry*, vol. 80, no. 3, pp. 217–231, 2006.

[46] J. Lloyd and J. A. Taylor, "On the temperature dependence of soil respiration," *Funct. Ecol.*, vol. 8, no. 3, pp. 315–323, 1994.

[47] D. Baldocchi *et al.*, "FLUXNET: A new tool to study the temporal and spatial variability of ecosystem–scale carbon dioxide, water vapor, and energy flux densities," *Bull. Amer. Meteorol. Soc.*, vol. 82, pp. 2415–2434, Sep. 2001.

[48] D. Baldocchi, "'Breathing' of the terrestrial biosphere: Lessons learned from a global network of carbon dioxide flux measurement systems," *Austral. J. Botany*, vol. 56, pp. 1–26, Sep. 2008.

[49] M. Reichstein *et al.*, "On the separation of net ecosystem exchange into assimilation and ecosystem respiration: Review and improved algorithm," *Global Change Biol.*, vol. 11, pp. 1424–1439, Apr. 2005.

[50] A. R. Desai *et al.*, "Cross-site evaluation of eddy covariance GPP and RE decomposition techniques," *Agricult. Forest Meteorol.*, vol. 148, pp. 821–838, Sep. 2008.

[51] N. Carvalhais *et al.*, "Identification of vegetation and soil carbon pools out of equilibrium in a process model via eddy covariance and biometric constraints," *Global Change Biol.*, vol. 16, no. 10, pp. 2813–2829, 2010.

[52] L. Guanter *et al.*, "Global and time-resolved monitoring of crop photosynthesis with chlorophyll fluorescence," *Proc. Nat. Acad. Sci. USA*, vol. 111, no. 14, pp. E1327–E1333, 2013.

[53] J. Joiner *et al.*, "Global monitoring of terrestrial chlorophyll fluorescence from moderate spectral resolution near-infrared satellite measurements: Methodology, simulations, and application to GOME-2," *Atmos. Meas. Techn.*, vol. 6, no. 2, pp. 2803–2823, 2013.

[54] C. Frankenberg *et al.*, "Prospects for chlorophyll fluorescence remote sensing from the orbiting carbon observatory-2," *Remote Sens. Environ.*, vol. 147, no. 5, pp. 1–12, 2014.

[55] G. R. van der Werf, J. T. Randerson, L. Giglio, L. Collatz, G. J. Kasibhatla, and A. F. Arellano, "Interannual variability in global biomass burning emissions from 1997 to 2004," *Atmos. Chem. Phys.*, vol. 6, pp. 3423–3441, Sep. 2006.

[56] Global Soil Data Task Group. (2000) "Global gridded surfaces of selected soil characteristics (International Geosphere-Biosphere Programme–Data and Information System)," Oak Ridge Nat. Lab. Distrib. Active Arch. Center, Oak Ridge, TN, USA, Dataset, Accessed Jan. 1, 2015. [Online]. Available: http://www.daac.ornl.gov doi:10.3334/ORNLDAAC/569.

[57] G. J. Hugelius *et al.*, "Estimated stocks of circumpolar permafrost carbon with quantified uncertainty ranges and identified data gaps," *Biogeosciences*, vol. 11, no. 23, pp. 6573–6593, 2014.

[58] E. G. Jobbágy and R. B. Jackson, "The vertical distribution of soil organic carbon and its relation to climate and vegetation," *Ecol. Appl.*, vol. 10, no. 2, pp. 423–436, 2000.

[59] F. A. Heinsch *et al.*, "Evaluation of remote sensing based terrestrial productivity from MODIS using regional tower eddy flux network observations," *IEEE Trans. Geosci. Remote Sens.*, vol. 44, no. 7, pp. 1908–1925, Jul. 2006.

[60] J. T. Randerson, M. V. Thompson, C. M. Malmstrom, C. B. Field, and I. Y. Fung, "Substrate limitations for heterotrophs: Implications for models that estimate the seasonal cycle of atmospheric CO_2," *Global Biogeochem. Cycles*, vol. 10, no. 4, pp. 585–602, 1996.

[61] A. Bartsch *et al.*, "Can C-band SAR be used to estimate soil organic carbon storage in tundra?" *Biogeosciences*, vol. 15, pp. 5453–5470, Sep. 2016.

[62] S. Unger, C. Máguas, J. S. Pereira, T. S. David, and C. Werner, "The influence of precipitation pulses on soil respiration—Assessing the 'Birch effect' by stable carbon isotopes," *Soil Biol. Biochem.*, vol. 42, pp. 1800–1810, Apr. 2010.

[63] L. Xu, D. D. Baldocchi, and J. Tang, "How soil moisture, rain pulses, and growth alter the response of ecosystem respiration to temperature," *Global Biogeochem. Cycles*, vol. 18, no. 4, pp. 1–10, 2004.

[64] T. Ohta *et al.*, "Effects of waterlogging on water and carbon dioxide fluxes and environmental variables in a Siberian larch forest, 1998–2011," *Agricult. Forest Meteorol.*, vol. 188, pp. 64–75, Sep. 2014.

[65] R. Reddy and R. D. DeLaune, "Adaptation of plants to soil anaerobiosis," in *Biogeochemistry Wetlands*. Boca Ranton, FL, USA: CRC Press, 2008, pp. 215–256.

[66] C. Beer *et al.*, "Terrestrial gross carbon dioxide uptake: Global distribution and covariation with climate," *Science*, vol. 329, pp. 834–838, Sep. 2010.

[67] M. Jung *et al.*, "Global patterns of land-atmosphere fluxes of carbon dioxide, latent heat, and sensible heat derived from eddy covariance, satellite, and meteorological observations," *J. Geophys. Res. Biogeosci.*, vol. 116, p. G00J07, 2010, doi: 10.1029/2010JG001566.

[68] Y. Yi, J. S. Kimball, L. A. Jones, R. H. Reichle, and K. C. McDonald, "Evaluation of MERRA land surface estimates in preparation for the Soil Moisture Active Passive Mission," *J. Climate*, vol. 24, no. 15, pp. 3797–3816, 2011.

Lucas A. Jones (S'06–M'17) received the Ph.D. degree in systems ecology from the University of Montana, Missoula, MT, USA, in 2016.

From 2010 to 2013, he was a NASA Earth System Science Fellow. He is currently a Post-Doctoral Scientist with the Numerical Terradynamic Simulation Group, University of Montana. He is the Lead Scientist and a Scientific Software Developer of SMAP Level 4 Carbon. His research interests include global land carbon and water cycle questions using data fusion and uncertainty analysis, combining information from microwave and other remote sensing data sources with land surface models.

Dr. Jones is a member of the American Geophysical Union.

John S. Kimball (M'08–SM'16) received the Ph.D. degree in bioresource engineering and geosciences from Oregon State University, Corvallis, OR, USA, in 1995.

He is currently a Professor of systems ecology with the University of Montana, Missoula, MT, USA. His research interests include the integration of ecological theory with satellite remote sensing for clarifying ecosystem structure and function from landscape to global scales.

Dr. Kimball is a member of the NASA Soil Moisture Active Passive (SMAP) Mission Science Team and a Principal Investigator of the SMAP Level 4 Carbon product.

Rolf H. Reichle received the M.S. degree ("Diplom") in physics from the University of Heidelberg, Heidelberg, Germany, in 1996, and the Ph.D. degree in environmental engineering from the Massachusetts Institute of Technology, Cambridge, MA, USA, in 2000.

He is currently a Research Physical Scientist with the Global Modeling and Assimilation Office, NASA Goddard Space Flight Center, Greenbelt, MD, USA. His research interests include land data assimilation, satellite-based remote sensing, and applications related to land–atmosphere interactions, weather prediction, and seasonal climate forecasting.

Nima Madani is currently pursuing the Ph.D. degree in systems ecology with the University of Montana, Missoula, MT, USA.

He is currently involved in the validation of Soil Moisture Active Passive Level 4 Carbon product using flux tower carbon network and other satellite products and observations including the solar-induced chlorophyll fluorescence. His research interests include terrestrial carbon cycle modeling, the remote sensing of global environmental change, the effects of extreme climate events on ecosystem productivity, and species–habitat relationships.

Joe Glassy is with Lupine Logic Inc., Missoula, MT, USA, and also with the Numerical Terradynamic Simulation Group, University of Montana, Missoula, MT, USA. He is the primary Software Engineer of SMAP Level 4 Carbon.

Joe V. Ardizzone is with the NASA Global Modeling and Data Assimilation Office (GMAO), Goddard Space Flight Center, Greenbelt, MD, USA. He is responsible for SMAP Level 4 Carbon and Level 4 Soil Moisture operations at GMAO.

Andreas Colliander (S'04–A'06–M'07–SM'08) received the M.Sc. (Tech.), Lic.Sc. (Tech.), and D.Sc. (Tech.) degrees from the Helsinki University of Technology (TKK; now Aalto University), Espoo, Finland, in 2002, 2005, and 2007, respectively. He is currently a Research Scientist with the Jet Propulsion Laboratory, California Institute of Technology, Pasadena. He is a member of the Science Algorithm Development Team for the Soil Moisture Active and Passive (SMAP) mission, focusing on calibration and validation of the geophysical products.

James Cleverly received the B.S. degree in biology from the University of Utah, Salt Lake City, UT, USA, in 1993, and the Ph.D. degree in biological sciences from the University of Nevada, Las Vegas, NV, USA, in 1999.

From 1999 to 2009, he was a Post-Doctoral Fellow and then a Research Assistant Professor with the Hydrogeoecology Group, University of New Mexico, Albuquerque, NM, USA. Since 2009, he has been a Research Fellow with the Terrestrial Ecohydrology Research Group, University of Technology Sydney, Sydney, NSW, Australia. He has authored more than 50 peer-reviewed articles. His research interests include ecohydrology and carbon relations of drylands, groundwater–soil–vegetation–atmosphere interactions, plant carbon and water relations, climatology and meteorology of extreme events, and agronomy.

Dr. Cleverly is a member of the Australian Meteorological and Oceanographic Society, the American Geophysical Union, and the American Meteorological Society. He received the Research Award from the New Mexico Riparian Council in 2003 and the Best Student Poster Award by the Physiological Ecology Section of the Ecological Society of America in 1996. He serves on the board of editors of the *Advances in Meteorology*, as a Science Director of the Australian flux network *TERN OzFlux*, and he served as an Expert Witness of an interstate water dispute settled by the U.S. Supreme Court in 2002.

Ankur R. Desai received the B.S. degree in computer science and environmental studies from Oberlin College, Oberlin, OH, USA, in 1997, the M.S. degree in geography from the University of Minnesota–Twin Cities, Minneapolis, MN, USA, in 2000, and the Ph.D. degree in meteorology from The Pennsylvania State University, State College, PA, USA, in 2006.

He is currently an Associate Chair and a Professor of the Atmospheric and Oceanic Sciences Department with the University of Wisconsin–Madison, Madison, WI, USA, where he holds the N. P. Smith Professorship of Climatology and also a Faculty Affiliate of the Nelson Institute Center for Climatic Research, Nelson Sustainability and Global Environment Center, and the UW Freshwater and Marine Sciences program. His research interests include micrometeorology, ecology, and how space and time scales influence ecosystem exchanges of greenhouse gases, energy, and momentum with the atmosphere.

Prof. Desai is a member of the American Geophysical Union, the American Meteorological Society, and the Ecological Society of America. He was a recipient of the AMS Clarence Leroy Meisinger Award. He served as the Chair of the AMS Committee on Agricultural and Forest Meteorology and an Editor of the AGU's *Journal of Geophysical Research*.

Derek Eamus is with the University of Technology Sydney, Sydney, NSW, Australia.

Eugénie S. Euskirchen is with the Institute of Arctic Biology, University of Alaska Fairbanks, Fairbanks, AK, USA.

Lindsay Hutley is with Charles Darwin University-Casaurina, Darwin, NT, Australia.

Craig Macfarlane is with CSIRO, Floreat, WA, Australia.

Russell L. Scott is with USDA Agricultural Research Service, Tucson, AZ, USA.